

Review

# Liquid Phase Calorimetric Method as a Tool for Acid Strength Measurements and Application to a Variety of Sustainable Catalysts

Deborah da Silva Valadares <sup>1</sup>, Juliene Oliveira Campos de França <sup>1</sup>, Roberto Chaves Fernandes <sup>1</sup>,  
Luiz Marcos Dezaneti <sup>2</sup>, Sílvia Cláudia Loureiro Dias <sup>1,\*</sup> and José Alves Dias <sup>1,\*</sup>

<sup>1</sup> Catalysis Laboratory, Asa Norte, Chemistry Institute, Darcy Ribeiro University Campus, University of Brasília, Brasília 70910-900, DF, Brazil

<sup>2</sup> Federal Institute of Education, Science and Technology of Goiás, Campus Valparaíso de Goiás, BR-040, km 6, Avenida Saia Velha, S/N, Area 8, Parque Esplanada V., Valparaíso de Goiás 72876-601, GO, Brazil

\* Correspondence: scdias@unb.br or silviadiasunb@gmail.com (S.C.L.D.);  
jdias@unb.br or josediadunb@gmail.com (J.A.D.); Tel.: +55-61-3107-3846 (J.A.D.);  
Fax: +55-61-3107-3900 (J.A.D. & S.C.L.D.)

**Abstract:** It has been about 36 years since the first published paper about the calorimetry and adsorption (Cal-Ad) method by Prof. Drago. These separated methods are very old and important characterization tools for different molecules and materials, as recognized in chemistry. The idea of coupling these two techniques arose from the need to have more information about the thermodynamic parameters of a catalyst. The Cal-Ad method provides a measure of the magnitude ( $K_i$ ), strength ( $-\Delta H_i$ ), and quantity ( $n_i$ ) of sites present in a catalyst. The original idea is based on the application of the donor-acceptor concept using the Electrostatic Covalent Model, ECW in the areas of catalysis and material chemistry. Particularly, enthalpy measurements of acidity are directly related to the activity of various catalysts in a variety of reactions. Currently, more than twenty-five catalysts have been carefully characterized by this method in addition to spectroscopic and other thermal methods. Thus, this review seeks to present the fundamentals of the method and show different applications of the characterized catalysts for a variety of reactions in order to use these data as an alternative to choose a catalyst for an acid-dependent type reaction.

**Keywords:** solid acids; calorimetry and adsorption (Cal-Ad) method; acidity; acid site strength; acid catalytic reactions



**Citation:** Valadares, D.d.S.; de França, J.O.C.; Fernandes, R.C.; Dezaneti, L.M.; Loureiro Dias, S.C.; Dias, J.A. Liquid Phase Calorimetric Method as a Tool for Acid Strength Measurements and Application to a Variety of Sustainable Catalysts. *Chemistry* **2023**, *5*, 1138–1170. <https://doi.org/10.3390/chemistry5020078>

Academic Editor: José Antonio Odriozola

Received: 29 March 2023

Revised: 29 April 2023

Accepted: 1 May 2023

Published: 9 May 2023



**Copyright:** © 2023 by the authors. Licensee MDPI, Basel, Switzerland. This article is an open access article distributed under the terms and conditions of the Creative Commons Attribution (CC BY) license (<https://creativecommons.org/licenses/by/4.0/>).

## 1. Introduction

### 1.1. Brief History of Calorimetry

Calorimetry is one of the oldest techniques used in chemistry and other areas of science. Many different philosophers and scientists have thought about the idea of heat and temperature, going back as far as the year 480 of the Common Era, although for centuries these concepts remained poorly understood. However, the work of the Scottish chemist Joseph Black (1761) established a clear distinction between those variables and because of that, he is considered the founder of the science of calorimetry. Subsequently, the next important mark was building the first calorimeter in 1798 by Antoine Lavoisier in collaboration with the mathematician Pierre Simon de La Place. Then, James Prescott Joule precisely measured the mechanical equivalent of heat (4.184 J per calorie of work to raise the temperature of one pound (lb) of water by one degree Fahrenheit (F)) by 1841. Simultaneously, in 1840, Germain Hess elucidated the important topic of thermochemistry, which is an expression of the principle of energy conservation for a system. Nevertheless, it took until 1870 for Pierre Berthelot to be credited with the fabrication of the first bomb calorimeter, a figure who was also credited with inventing the concept of exothermic and

endothermic reactions. These facts represent the origins of the first modern calorimeters and can be read about in a very interesting article published by Meschel [1].

### 1.2. Brief History of Adsorption

The appearance of the adsorption phenomenon has risen from ancient times, citing some of the earliest researchers such as Scheele, Priestley, and Fontana in 1773–1777. At the end of the eighteenth century, the term adsorption, which is distinct from absorption, was introduced by Emil du Bois-Reymond and Heinrich Kayser in 1881 [2]. Adsorption is the interaction between molecules and a solid surface (external or internal on a wall porous surface) due to the existence of uncompensated attractive forces. On the other hand, absorption is related to the whole volume (bulk) of the solid. Since the adsorption process often precedes absorption, and sometimes it is not obvious to see the distinction, the term sorption was presented by James W. McBain (1909) to encompass both phenomena. The adsorption process can be classified as physisorption (characterized by non-specific interactions, e.g., van der Waals forces) or chemisorption (characterized by specific interactions, e.g., covalent bonding, electrostatic forces). The description of adsorption is generally described through isotherm curves, i.e., the amount of the adsorbed molecule (adsorbate) on the solid (adsorbent) as a function of its content at a constant temperature. Irving Langmuir was the first researcher to describe in detail the monolayer-based theory using a scientifically based adsorption isotherm (1916–1918), even though Herbert Freundlich in 1907 and Michael Polanyi in 1914 had been pioneers in these emerging ideas before. It is claimed that at least fifteen different isotherm models have been developed to date [3]. Adsorption processes, and particularly the Langmuir model, have been impactful in different fields of science and technology today, which is fully described in the recent and interesting work of Swenson and Stadie [2].

## 2. Brief Overview of Solid Acidity Strength

Basically, there is an overlap between the concept of acidic solids and heterogeneous catalysts. Its development is intimately related to the progress of catalysis in the twentieth century to enhance the production of fuels from oil hydrocarbons and important chemical molecules to work as intermediates in industry. Although knowledge of the catalytic behavior of solids is considered a natural phenomenon, a systematic study is mandatory to develop it as a science and technology subject.

The nature of active sites in any catalytic system is essential to understanding and designing new materials for heterogeneous catalysis. In this sense, the classical concepts of acids and bases are mandatory to create a minimum architecture for the functional utility of the desired solid acid. The definition of acidity for a material is interdependent with the possible base used to probe the relative acid-base interaction. There are several definitions of acidity in the literature (e.g., Arrhenius, Brønsted-Lowry, Lewis, solvent system, Lux-Flood, Usanovich, hard-soft acids and bases, electrostatic-covalent acid-base interactions, Hammett equation and super acidity, gas-phase proton affinity), which are basically discussed in many classical books of inorganic chemistry [4–8]. For solids, the definitions of Brønsted and Lewis are by far the most important and applied in relation to the properties of solids. According to the classical definition in solution, a Brønsted acid is a species that releases a proton to another one, which acts as an acceptor of this proton and behaves like a base. Likewise, Lewis acid is a substance that accepts an electron pair to form a chemical bond, whereas a base is just an electron-donating substance. As it is well known, the Lewis definition is not restricted to a solution or a proton transfer reaction and even though the definition of Lewis encompasses the Brønsted, chemical reactions that involve a proton transfer are conveniently treated using the Brønsted-Lowry concept.

Surface acidity of solids has been debated and described in the literature for decades but can be consensually considered as dependent on the nature of the bond holding its own solid. The solid surface will present some kind of defect related to the exposed atoms of the final layer, which are subjected to valence or coordination unsaturation. As a result,

these atoms (or sites) have high free Gibbs energy and will seek stabilization by adsorption of molecules from the environment (e.g., H<sub>2</sub>O, CO<sub>2</sub>, O<sub>2</sub>). The recovery of the original unsaturation can be obtained by desorption of adsorbed species under heating or vacuum. Thus, the activity of this surface is related to this reversible process of adsorption-desorption of different molecules at the unsaturated-saturated surface, which, in turn, is dependent on the environmental composition as well as the temperature and pressure of the medium. In that sense, the main reason for the difficult characterization of solid surfaces arises from the variety of reactivity conditions under which these surfaces can interact with possible substrates under a reactional medium (e.g., gas-solid, liquid-solid). Nevertheless, one should be aware that a possible classification of solids into acids (or bases) may be not so straight in several cases because of the large heterogeneity of solid surfaces. These very succinct ideas and discussions are intended more to compel the reader to go deeper into the many excellent reviews about the acidity of solids and their characterization methods [9–19]. The next section deals with some of the classical methods for the characterization of solid acid strength. Nonetheless, there is no intention to revise such methods, but it will only allow the reader to be aware of the fundamentals of each one and provide a few references for further research.

### 2.1. Base-TPD (Temperature Programmed Desorption)

TPD is associated with pre-adsorption of a base probe molecule (e.g., pyridine, NH<sub>3</sub>, amine) on the solid acid and further desorbed under a controlled temperature condition. The main detection systems are mass changes (TPD-TG), thermal conductivity (TPD-TC) and mass spectrometry (TPD-MS). This has been extensively used to identify the acid sites for their strength, distribution (or density), and nature. The analysis involves the area under the curve of the TPD profile, which measures the total quantity of the acid sites. In addition, the peak temperatures can be used as an acid site strength measurement. Moreover, usually it takes a range of temperatures, since the peaks are normally large, for quantification of strong, medium, and weak sites on the solid. Lately, NH<sub>3</sub>-TPD is one of the most commonly used methods for acid strength characterization. This might be attributed to the ease and automation of applying the method. Nonetheless, some issues are argued in the literature about the feasibility of this probe to measure Brønsted acid site strength. However, it can be anticipated that a combination of thermal desorption and spectroscopic analysis is powerful for acidity characterization. The reader can consult some of the cited references for further study on applications of this subject [20–28].

### 2.2. Multinuclear Solid-State Nuclear Magnetic Resonance

Solid-state nuclear magnetic resonance (MAS NMR or SS NMR) spectroscopy is one of the most powerful techniques, considered investigative at the atomic scale, to provide evidence about the structure and the dynamics of processes occurring in the analyzed materials [29,30]. To achieve such a position, high-resolution development in the solid-state NMR was mandatory and reached at the end of the 1970s [31]. Practically all elements in the periodic table have at least one magnetically active isotope with nonzero nuclear spin, which is a requisite to be active in an NMR experiment. Two nuclear parameters (gyromagnetic ratio and natural abundance) are essentials to ascribe the relative receptivity of a nucleus and hence its sensitivity. As a result, the NMR technique is applicable to many different elements not only in compounds but also materials [32].

Particularly, in the study of catalysts the understanding of framework structures, catalytically active sites (and their important parameters, i.e., nature, distribution, concentration, strength) and intermolecular interactions can be addressed by multinuclear NMR [33]. Currently, there are state-of-the-art SSNMR techniques that improve the structural and quantitative characterization of catalysts including many nuclei (e.g., <sup>1</sup>H, <sup>13</sup>C, <sup>27</sup>Al, <sup>29</sup>Si, <sup>31</sup>P). These methods include the original single pulse, under the magic angle rotation with proton decoupling experiment and more advanced ex and/or in-situ pulse-field-gradient, variable temperature, double resonance, two-dimensional (2D) correlation,

homonuclear correlation, and double-quantum (DQ) or multiple-quantum (MQ) coherences spectroscopies [32–35]. Thus, with these improved methods, new insights have been provided for different heterogeneous catalysts at structural and acidic levels. A few examples in the literature involving the most popular nuclei will be offered to the reader that could be useful for the design and characterization of solid acid catalysts.

The characterization of acidic OH groups by  $^1\text{H}$  SS NMR is of major interest in the determination of acidity for solid acids such as zeolites and other oxides [36,37]. The acidity can be determined by the strength and concentration of hydroxyl protons. The first can be derived from  $^1\text{H}$  chemical shift ( $\Delta\delta_{1\text{H}}$ ), which in principle is dependent on the magnitude of the shift, i.e., the larger the chemical shift the higher the acid strength, whereas the second is derived from the signal intensities of the hydroxyl protons. It may be difficult knowing about the straight relation between intrinsic strength and the chemical shift if hydrogen bonds are involved in such a system. In this case, the adsorption of a probe molecule at the acidic OH group is important to characterize Brønsted sites. The same is valid for Lewis sites, which are preferentially studied by the same process. One advantage of SS NMR is that it can be quantitative if an internal or external intensity standard is used to calculate the number of acid sites. The reader should read excellent reviews involving  $^1\text{H}$  SS NMR, employing zeolites as solid acids [33,36,37].

The structure of aluminosilicates and other catalysts containing silicon and aluminum can be conveniently studied by  $^{27}\text{Al}$  and  $^{29}\text{Si}$  SS NMR. The strength of Brønsted acidity primarily depends on the concentration and the chemical environment of the Al (e.g., coordination, position in or out of the framework), which is, in turn, dependent on the framework and total Si/Al ratio of the material. Properties such as hydrophilicity, hydrophobicity, and stability of zeolites are related to the concentration and distribution of Al atoms, which is dependent on the difference in the stabilities between Si–O and Al–O bonds that are intricate with the affinity of protons to water molecules. The literature is rich in papers using SS NMR of silicon and aluminum to characterize and correlate the properties of zeolites after tailoring their acidities during synthesis or post-synthesis of these materials to different applications. The reader should be aware of various recent reviews about SS NMR of  $^{27}\text{Al}$  and  $^{29}\text{Si}$  [38–42].

Another approach to characterize the acidity strength of Brønsted sites is to use weakly basic probe molecules (e.g., acetonitrile, acetone, perchloroethylene or trimethylphosphine oxide) that can interact by hydrogen bonding [37]. The interaction generates low-field shifts ( $\Delta\delta$ ) on the  $^1\text{H}$  SS NMR spectra of the hydroxyl species or in the functional groups of the probe molecules (e.g.,  $^{13}\text{C}$ ,  $^{15}\text{N}$ , or  $^{31}\text{P}$  SS NMR). One of the difficulties for  $^{13}\text{C}$  and  $^{15}\text{N}$  is that the adsorbed probes should be enriched to obtain a good spectrum. This is not necessary to obtain  $^{31}\text{P}$  SS NMR spectra. Thus, the method using triethylphosphine oxide (TEPO) or trimethylphosphine oxide (TMPO) is turning into one of the most popular while using adsorbed molecules to measure acidity by SS NMR [43–46]. For instance, Osegovic and Drago [43] found that the chemical shift of  $^{31}\text{P}$  MAS NMR of TMPO correlates with the heat of adsorption onto the acid sites of the (silica-gel) $_n\text{Sb}^{\text{V}}\text{Cl}_3$  catalyst. Zasukhin et al. [47], in a recent article, studied adsorbed alkyl-substituted phosphine oxides (trimethylphosphine oxide (TMPO), tri-*n*-butylphosphine oxide (TBPO), and tri-*n*-octylphosphine oxide (TOPO)) on BEA zeolites. The proposed methodology was able to quantitatively measure the number of Brønsted and Lewis sites, as well as the number of internal and external silanol groups. In addition,  $^{31}\text{P}$  SS NMR has been used to perform structural studies of heteropolyacids (HPA) and their derivatives (e.g., salts, supported HPA) [48–52]. Therefore, the presence of one or more Keggin species (free or under direct interaction on a support surface), as well as decomposition products, can be well distinguished by this technique.

### 2.3. FT-IR of Base Adsorption

Infrared spectroscopy (IR) is based on the capacity of molecules to change their normal vibrations and hence dipole moments by absorption of photons in the infrared range (typically between  $14,000\text{--}10\text{ cm}^{-1}$ ), and thus change their discrete levels of rotational

and vibrational energy [53]. IR is one of the most popular and affordable characterization methods in chemistry. The first affordable infrared spectrometer of commercial origin dates from 1957 (Perkin-Elmer, model 137 Infracord, Shelton, CT, USA) [54]. After more than 65 years, Fourier transform IR (FT-IR) remains the most widely used, and typically one of the most effective, spectroscopic methods for the chemical surface characterization of heterogeneous catalysts [28,55,56].

The infrared spectra of adsorbed probe molecules (e.g., pyridine,  $\text{NH}_3$ ,  $\text{CO}_2$ ,  $\text{CO}$ ,  $\text{NO}$ ) furnishes important information about the active sites on a catalyst and thus the acidity of solid acids. The pioneering work by Parry [57], Basila et al. [58], and Hughes et al. [59] showed that the pyridine molecule is capable of simultaneously determining the concentration of Brønsted and Lewis acid sites. It also could distinguish hydrogen bonding type sites [57]. The infrared region between 1400 and 1700  $\text{cm}^{-1}$  displays clear differences in the pyridine coordinately bonded (Lewis) to the pyridinium ion (Brønsted) adsorbed on a solid acid surface. There are a number of papers in the literature dealing with quantitative IR measurements involving pyridine and other molecules, which have proved to be appropriate for the investigation of the accessibility of various solid acids (e.g., zeolites). The reader can take a deeper look at some of the references provided here to apply this method to different catalysts [60–62].

It should be mentioned that hydroxyl groups on the surface of catalysts are very important as active centers, and FT-IR (especially DRIFTS, diffuse reflectance infrared Fourier transform spectroscopy) under controlled atmospheric conditions is fundamental to characterize their interaction with probe molecules. Usually, a possible formation of H-bonds between the molecule and O-H group or a chemical reaction with that group (e.g., redox, exchange) is the expected information that could be obtained. Thus, a comprehensive review of this subject is indicated [63].

#### 2.4. Gas Phase Adsorption Microcalorimetry

The important phenomena of adsorption, reaction, and desorption that take place on a solid surface are controlled by the thermodynamics of the energetics of these processes. The fundamentals of physical-chemical aspects of adsorption are very well described in a book by Adamson et al. [64], which is intended for readers new to this area. Adsorption is recognized as an essential part of catalytic studies [64–66]. The catalytic properties of the solid surface are essentially determined by the energetics of the surface events. The nature of both the molecule (adsorbate) and the solid material (adsorbent) determines the strength of the interaction between them. The magnitude of this interaction can be either specific or non-specific, which gives rise to measurements that demand the accuracy of the heat evolved, as well as on the amounts of adsorbed gas [67]. The use of a suitable calorimeter is considered the most reliable method to measure accurately the heat evolved. One of the most utilized systems uses Tian-Calvet heat-flow microcalorimeters as a high-sensitivity apparatus [68]. The equipment is constructed under a differential setup, i.e., a vessel containing the sample and others (usually empty) acting as a reference, which avoids any heating measurement being compensated due to the interaction of the gas with the solid surface. Generally, the equipment allows the heat of adsorption to be measured under a constant temperature ( $25\text{ °C} < T < 400\text{ °C}$ ). The interpretation of the isotherm curves (average differential heat versus adsorbate coverage) can obtain important data about the strength and the number of acid sites in a catalyst [65–68]. These microcalorimetric measurements have been used to characterize a number of catalysts in the literature (e.g., silica-alumina, zeolites, HPA, mesoporous silica) making use of different probe molecules (e.g.,  $\text{NH}_3$ , pyridine, amines,  $\text{CO}_2$ ,  $\text{SO}_2$ ) [69–77]. It also should be mentioned that many authors in the literature use liquid phase calorimetry to estimate the acidity of various catalysts, which is possible to discriminate the acid site strength accurately.

### 3. The Calorimetry-Adsorption (Cal-Ad) Method Proposed by Prof. Russel Drago

#### 3.1. Fundamental Aspects

The largest applications of donor-acceptor concepts may be ascribed to the areas of materials and catalysis [78]. The Electrostatic-Covalent (ECW) model was proposed in 1965 by Drago and Wayland, in which each acid and base is described by two parameters (E-electrostatic and C-covalent), according to Equation (1):

$$-\Delta H = E_A E_B + C_A C_B + W \quad (1)$$

where,  $\Delta H$  is the enthalpy of the formation of a Lewis acid-base adduct,  $E_A$  and  $C_A$  are characteristic parameters of the acid,  $E_B$  and  $C_B$  are characteristic parameters of the base, and  $W$  is an energy constant associated with a particular reactant (acid), regardless of the reaction it participates in (e.g., an acid dimmer such as  $Al_2Cl_6$  that has to break bonding before reaction with a base). This description of acid (acceptor) and base (donor) properties is parallel to the bonding models of Pauling and Mulliken [79,80].

Drago and many associates (especially graduate students) proposed several ways to express reaction enthalpies in terms of acidity and basicity parameters. For homogeneous systems, the ECW model was demonstrated to be very reliable, but for heterogeneous systems, it was more complex, however, it was addressed in different catalysts in liquid-solid equilibria, which is also important for applications in adhesion and material chemistry [78,81]. Due to the lack of a technique that furnishes a complete description of the thermodynamic parameters of solid acid, the Cal-Ad (coupling of calorimetry and adsorption measurements) could be an alternative to supply these parameters.

The Cal-Ad method is employed using two independent experiments. It is described here as a base reacting to a solid acid, but it can be the opposite (an acid reacting to a solid base). The calorimetric experiment measures the heat evolved upon incremental additions of an adsorbate (base) in a solution to a slurry of the solid (acid) in the same solvent during a calorimetric titration. This heat depends on the equilibrium constant ( $K$ ), the enthalpy of interaction ( $\Delta H$ ), and the number of sites ( $n$ ) on the solid. The interval between additions is about 3–5 min. The obtained data generates an isotherm of total heat evolved versus the total moles of the base added since the concentration of the base solution added is known for each addition.

The adsorption experiment is conducted, independently, using the same mass and volume of solvent in the slurry used for the calorimetry. The same incremental volume added to the base solution should be kept in order to parallel the equilibrium achieved in the calorimetric experiment. After the addition of the base and stirring for 3–5 min, the stirring is interrupted to let the solids settle, and an aliquot of the solution is taken out and replaced by the same volume of the pure solvent. Then, the next addition is made, and the procedure is repeated up to the end of the titration. The base concentration is obtained using an analytical method (e.g., UV-Vis spectroscopy). The remaining base in the solution is recalculated after each sample is removed. Since the total base added is known and the free base is obtained by the adequate method, the base adsorbed on the solid is calculated by the difference. The data generates an isotherm of the moles of the base adsorbed versus moles of the base in solution.

The use of the solvent should also be justified. In principle, the strength of bonding between the solid acid and a base should be only based on donor-acceptor interaction. Thus, any solvent that has a specific interaction with both (solid acid and/or base) should be avoided or the specific effect should be factored out. If a poorly interacting solvent is chosen, those specific interactions are absent, and it is not necessary to be considered. Generally, the ECW system is used as solvent  $CCl_4$ , hexane or cyclohexane, which agrees with those weak interactions. In these solvents, the dispersion interactions among the solvent, the solid acid, and the base will take place. In this sense, the Cal-Ad method is conducted using a hydrocarbon solvent whose molecules are close in molecular mass to those of the donor to minimize these dispersion interactions. The reaction of the solvated base with the

solvated solid acid takes place by displacement. In earlier studies by Drago et al. [82–85], it was shown that the product and reactant nonspecific dispersion interactions cancel out and do not contribute to enthalpies measured in solution, which differ from gas phase donor-acceptor interactions (e.g., proton affinities, which are not displacement reactions) that has dispersion and donor-acceptor contributions. Therefore, the use of such solvents is preferable to account only for specific donor-acceptor interaction heating measurements.

It is important to understand that the Cal–Ad method measures the enthalpy of a base-displacement reaction, which is different from the equivalent experiment in gas–solid calorimetry that measures an adduct formation between the base and the solid. A comparison of the results of gas–solid calorimetry using HZSM-5 as a catalyst interacting with pyridine has been demonstrated to be a measure of the weighted average Cal–Ad enthalpy of pyridine interaction [86]. Using a Born–Haber thermodynamic cycle (Hess’s law) with the appropriate values, it was possible to show that enthalpies derived from gas–solid calorimetry are an average of the two enthalpies of the interaction of pyridine with the two acid sites obtained by the Cal–Ad method.

Another important issue to address is the time interval between incremental addition of a base. The time is measured by two straight ramps (Figure 1) of the calorimetric apparatus. After the addition of a base, the heat evolved gives a signal related to the temperature increase in the system, and by the time the temperature stabilizes a second straight line is observed. In the studied solids, it was observed that between 3 and 5 min was enough to have this behavior, and this was taken as the equilibrium reached time. Thus, many results may pertain to the initial donor-acceptor process and the term equilibrium should be understood as it, and not necessarily as a true final equilibrium for the system [87].

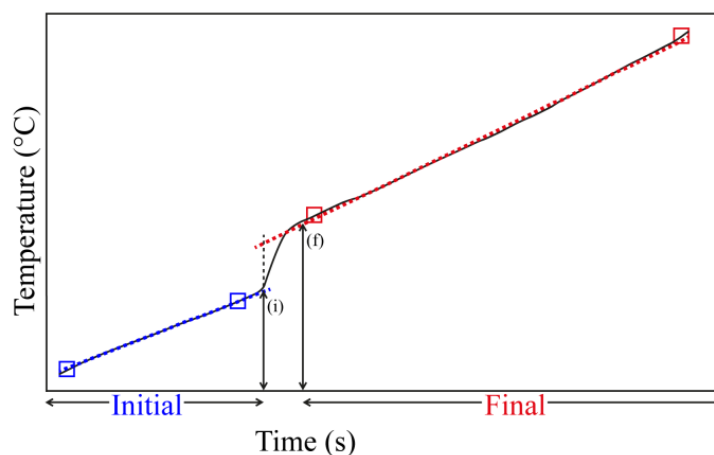


**Figure 1.** Example of an incremental addition of a base (e.g., pyridine) using the magnetic stirring system in the calorimeter, showing the initial and final interval time before a new addition. (i) time of the base injection; (f) time where the system reaches the maximum increment of temperature.

### 3.2. Experimental Procedure

The current microcalorimetric titrations are conducted in a modified (magnetic stirring system) isoperibol solution calorimeter (ISC, Model 4300, Calorimetry Sciences Corporation, Linden, UT, USA). This is a technique in which the temperature of a reaction vessel in a constant-temperature system is examined as a function of time. The equipment is coupled to a computer, running under Windows XP, and the experiments are registered according to the provided software (Hart ISODESC and ISOPER programs). The catalyst should be thermally treated, according to the desired conditions, before measurements. Then the catalyst is moved to a glove box under  $N_2$  (99.99%, White Martins/Praxair, Brazil), weighed (e.g., 0.5 g), and transferred to the calorimetric cell (e.g., 50 mL), followed by the addition of 50 mL of anhydrous cyclohexane (usually, fresh distilled over  $P_2O_5$ ). In a glove bag filled with  $N_2$ , a calibrated gas-tight syringe (Hamilton, NV, USA, 5 mL) is filled with a known concentration of pyridine solution in cyclohexane (e.g.,  $0.1000 \text{ mol L}^{-1}$ ). Later, both

the cell and syringe are inserted into the calorimeter holder, which is immersed in a thermal bath regulated at a desired temperature (e.g., 25.0000 °C). Before any experiment, the system is allowed to equilibrate (~1 h). The addition of the pyridine solution is performed incrementally (e.g., 0.1 mL), using the injection system of the calorimeter. After each addition of pyridine, the heat evolved from its reaction with the solid in suspension is measured, considering the initial and final baseline observed in the software (Figure 1). The interval between additions was previously tested (mostly, from 3 to 5 min), which was sufficient for the system to equilibrate. The heat for each addition is calculated using the equivalent energy of the system, which is obtained from a calibration curve performed before and after each complete titration. The heat of the diluted base (pyridine) added to cyclohexane should be measured separately to make sure it can be considered negligible. The experimental conditions are adjusted to measure the highest heat evolved from different runs. Then, each titration is typically repeated two to three times. A schematic of the calorimeter is shown in Figure 2.

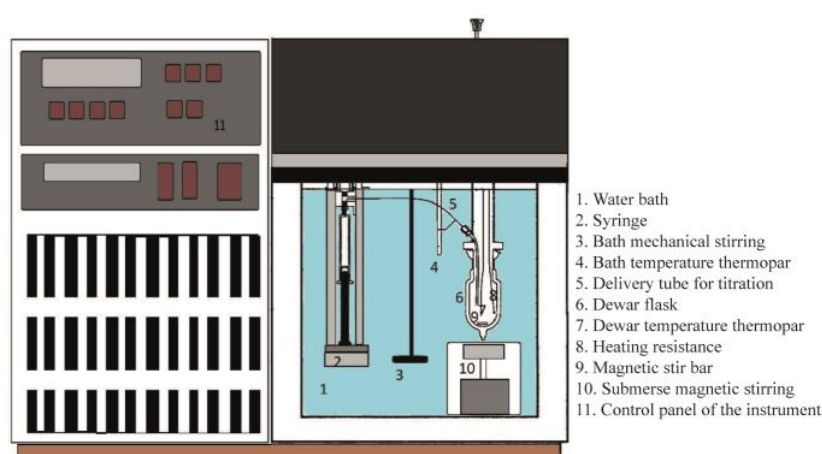


**Figure 2.** Representation of the calorimeter used in the current Cal-Ad titrations [88].

The present adsorption experiment is conducted in the following apparatus (Figure 3). It uses 0.5 g of solid that is added to a sealed three-neck round-bottom flask followed by 50 mL of anhydrous cyclohexane. Both operations are conducted inside a glove box. The addition of the base (e.g., pyridine solution) is performed using an automatic burette from Metrohm (model Dosimat 665, Herisau, Switzerland) in a room under the temperature of 25 °C. The added incremental volumes must be the same as for the calorimetric experiment (required by the Cal-Ad method). After each addition, a 1 mL sample of the solution is taken out from the flask and placed into a quartz cell of 1 cm pathlength. One milliliter of cyclohexane is placed back into the flask in order to keep the volume constant. These operations use a gas-tight syringe (Hamilton, NV, USA, 1 mL). The absorbance of pyridine is measured at 251 nm using a UV-Vis spectrophotometer (Beckman DU-650, Indianapolis, IN, USA), and to determine its equilibrium concentration in solution a previous analytical curve is prepared. For other bases such as 2,6-di-tertbutylpyridine (258 nm) and 2,6-lutidine (265 nm), the same procedure is followed for measurements. The amount of the base adsorbed by the solid is calculated by the difference between the known added base solution and that in equilibrium in the solution. Parallel to the calorimetric experiment, the adsorption experiment is also checked for diffusion constraints, and it was observed that for standing times of about 3 to 5 min there is no variation in the absorbance measurement. Thus, under these optimized conditions, the experiment is repeated two to three times.

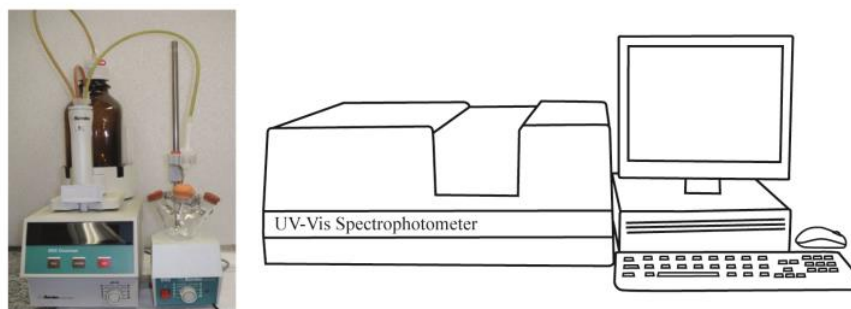


**Figure 3.** Experimental setup to perform the adsorption measurements.

### 3.3. Cal-Ad Analysis

The heat evolved upon the additions of a base in a slurry of the solid acid depends on the equilibrium constant ( $K$ ), the enthalpy of interaction ( $\Delta H$ ), and the number of sites ( $n$ ) on the solid. Thus, it is mandatory that the concentration of a base and the ratio  $V/g$  where  $V$  is the volume of solution (liter) and  $g$  is the mass of solid (gram), be the same in both experiments, i.e., calorimetry and adsorption. The approach is that a multiple-site Langmuir-type equation will describe both experimental isotherms (calorimetric and adsorption). On account of experimental limitations, generally, a model with one to three sites can fit both isotherms (frequently, it can properly differentiate two sites), and the use of very dilute solutions of a base (e.g., pyridine) is especially important. The original Cal-Ad methodology fitted the adsorption data first to generate the concentrations of the base in solution for the subsequent fit of the heat evolved [87,89]. However, when porous solids are used, eventually a quantity of a base that will saturate at least 60% of site two may be required since it is necessary to resolve the contributions of sites one and two to a  $-\Delta H$  average. Porosity leads to a large  $K$  for binding enthalpy even when  $-\Delta H$  is small, so the original Cal-Ad procedure had to be modified [78,89,90]. For zeolites (e.g., HZSM-5), detectable quantities of base (pyridine) are not observed in the solution until 0.1 mmol of pyridine has been added [90]. Thus, a new calculation is currently achieved for any solid acid.

### 3.4. Cal-Ad Calculations

An adsorption isotherm is constructed from the adsorption titration experiment that has the same range of base concentrations used in the calorimetric titration. The best-fit isotherm is calculated using a modified simplex routine designed to solve the following Langmuir-type equation (Equation (2)):

$$S_{TB} = \Sigma (n_i K_i [B]) / (1 + K_i [B]) \quad (2)$$

For a solid with  $i$  sites,  $S_{TB}$  = the total number of moles of base adsorbed per gram of solid;  $n$  = the number of moles of site  $i$  per gram of solid ( $\text{mol g}^{-1}$ );  $K_i$  = the equilibrium constant of binding at site  $i$  ( $\text{mol}^{-1} \text{L}$ );  $[B]$  = the equilibrium concentration of base in solution ( $\text{mol L}^{-1}$ ).

The calorimetric titration provides the heat evolved after base addition and only the total concentration of base added is known. Thus, the total number of moles of the base on the solid ( $S_{TB}$ ) is related to the total concentration of base added ( $[T]$ ,  $\text{mol L}^{-1}$ ), according to Equation (3):

$$S_{TB} = ([T] - [B]) V / g \quad (3)$$

where  $V$  = the volume of solvent used in the experiment (L);  $g$  = mass of solid used (g). Substituting Equation (2) into Equation (3), the following equation is obtained (Equation (4)):

$$([T] - [B]) V / g = \Sigma (n_i K_i [B]) / (1 + K_i [B]) \quad (4)$$

The preliminary estimate of  $K_i$  and  $n_i$  is obtained with data from the adsorption experiment. An estimate for  $\Delta H_i$  can be obtained by the limiting reagent approximation (i.e., using the heat evolved in the addition of a base divided by the total added). Then, they are used to calculate [B] from the calorimetric experiments using Equation (5):

$$h/g = \sum (n_i K_i [B] / (1 + K_i [B])) \Delta H_i \quad (5)$$

where  $h$  is the sum of the heat evolved (cal) from the calorimetric titration;  $g$  is the mass of solid (g); [B] is the concentration of the base in solution at equilibrium ( $\text{mol L}^{-1}$ );  $n_i$  is the number of each different site ( $\text{mol g}^{-1}$ );  $K_i$  is the equilibrium constant for each site ( $\text{mol}^{-1} \text{L}$ ); and  $\Delta H_i$  is the enthalpy of reaction with the base for each site on the solid ( $\text{kcal mol}^{-1}$ ). However, since the calorimetric titration does not measure the equilibrium concentration in the solution, this information is obtained through a polynomial series, according to Equation (6):

$$(V/g) [T] = x^n [B]^n + x^{n-1} [B]^{n-1} + x^{n-2} [B]^{n-2} + x^{n-3} [B]^{n-3} + \dots \quad (6)$$

where  $(V/g)$ ,  $[T]$ , and  $[B]$  have the meaning already explained. The polynomial is one degree higher than the number of sites (e.g., for one site, it uses a second-degree polynomial; for two sites it uses a third-degree polynomial). Thus, the  $x^n$  terms have the following adjustment:

$$\text{One site: } (V/g) [T] = x^2 [B]^2 + x [B]$$

$$\text{where: } x^2 = (V/g) K_1; x = n_1 K_1 - (V/g) K_1 [B] + (V/g)$$

$$\text{Two sites: } x^3 = K_1 K_2 (V/g); x^2 = n_1 K_1 K_2 + n_2 K_1 K_2 - (V/g) K_1 K_2 [T] + (V/g) K_1 + (V/g) K_2; \text{ and } x = n_1 K_1 + n_2 K_2 - (V/g) K_1 [T] - (V/g) K_2 [T] + (V/g).$$

As stated before, the first estimates of  $n$ 's and  $K$ 's are obtained from Langmuir adsorption data (Equation 2). The data adjusted to the model consist of the number of moles adsorbed and equilibrium concentration in solution (adsorption isotherm), and the sum of the heat and equilibrium concentration in solution (calorimetric isotherm). These  $n$ 's and  $K$ 's are then used in the polynomial expression to recalculate the concentrations of the base in solution for those systems too dilute to measure, as already described, and refit the combined calorimetric and adsorption data. This procedure is repeated until the  $n$ 's and  $K$ 's converge within the limit error of the program. Optimization of the parameters ( $n_i$ ,  $K_i$ , and  $\Delta H_i$ ) is performed using a non-linear least squares program with a Simplex computational routine. The Simplex method was developed by George Dantzig in 1946 and makes it possible to systematically (computationally) determine the optimal value of the objective function [91]. The original computer program was written in Fortran 77 by Ngai M. Wong and further enhancements were designed by Charles Edwin Webster (both PhD and former Drago's graduate students from UF). Based on the final values of  $K_i$  and  $\Delta H_i$ , it is possible to calculate the free Gibbs energy ( $\Delta G_i$ ) and the entropy ( $\Delta S_i$ ):

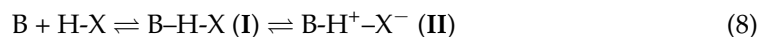
$$\Delta G_i = -\log(K_i) = \Delta H_i - T \Delta S_i \quad (7)$$

It should be noted that the original Cal-Ad data for enthalpy is  $\text{kcal mol}^{-1}$ , but all measurements were converted to SI units ( $\text{kJ mol}^{-1}$ ) multiplied by 4.184 in this review for convenience. Errors associated with the enthalpy measurements are about  $\pm 0.2$  to  $0.5$  kcal. By the time Drago developed the Cal-Ad method [87,89,92–94], it could be anticipated that its application would elucidate the thermodynamic parameters for catalysts and make use of a base (e.g., pyridine) as a reference, and that it would generate a relative scale of strength for solid acids. Thus, the consequent donor-acceptor enthalpy data provide a scale of solid acidity that is temperature independent from room temperature up to  $200$ – $300$  °C, which are those at which catalysts are commonly used. In addition, the correlation of Cal-Ad acidity ( $\Delta H$  or  $n$ ) with the catalytic activity could be used to establish the threshold acidity and choice of optimum solid acidity needed for acid-catalyzed reactions that would be an important tool in catalyst selection and design. Thus, in the next section a succinct

presentation of the different solid acid catalysts, whose characterization was by Cal-Ad, and some of their applications will be presented.

In some cases, it was only possible to obtain an estimate of the average enthalpy of the most important sites because of problems in the experimental apparatus at the time of the respective publication of the work. In these cases, for a model with two sites, the curve of heat evolved versus base (Py) added was taken in two linear portions, which were fitted by linear regression. The enthalpies ( $\Delta H_1$  and  $\Delta H_2$ ) were obtained from the slope of each regression. For the calculation of the number of sites ( $n_1$  and  $n_2$ ), it was obtained from selected enthalpy ranges. Two lines were proposed and split dividing the points. The choice of where one curve ends ( $n_1$ ) and another begins ( $n_2$ ) was calculated by linear regression of the points. When a point was added to the curve and a deviation from linearity was observed ( $r^2$  moves away from point one), the point was considered to belong to the other curve (the other acidic site, i.e.,  $n_2$ ).

It is also important to clarify the terminology we used for the sites [90]. Lewis acid site is related to an acceptor center on the catalyst (e.g., aluminum, niobium, metal). Brønsted site and hydrogen bond site are used to differentiate the products of a reaction. Considering pyridine as the reference, if it is bonded to the site without proton transfer to pyridine (i.e., not forming pyridinium), it will be called a hydrogen bond site. Conversely, if the proton is transferred to pyridine (i.e., forming pyridinium) it will be called a Brønsted site. Note that it is essential to understand that the same Brønsted site could function as a strong hydrogen bond site toward a weak donor, and vice-versa, i.e., any hydrogen bond site could act as a Brønsted site if a strong enough base is employed. The equilibria frequently described in solution (Equation (8)) are also relevant for solid acids (HX) in a reaction with a base (B) [95]:



where (I and II) show the hydrogen bond adduct whose equilibria will be displaced according to the nature and strength of B and H-X.

#### 4. Applications of Cal-Ad in the Characterization of Different Catalysts

##### 4.1. Catalysts Characterized Earlier by Dragos's Group

The first formal application of the Cal-Ad method to a heterogeneous catalyst involved a study of 5 wt.% palladium oxide supported on carbon (5 wt.% PdO/C) by Lim et al. [87]. The thermodynamic data for the adsorption of pyridine, N-methylimidazole (N-MeIm), and dimethylcyanamide (DMCA) using cyclohexane as the solvent in a slurry demonstrated important information about donor-acceptor bond energies of adsorption of these bases. The adsorption isotherm clearly revealed that more than one type of site was present on the solid (using a Langmuir model), as well as how the adsorption dependence on the time indicated that a fast equilibrium is established in this system that involves Lewis acid-base reactions, followed by a slower reaction involving less accessible sites. Thus, all the results regarded as equilibrium should be understood as the initial coordination of the base with the surface and not as the true (final) equilibrium for the system. The data analysis indicated that there are at least two acceptor sites on the palladium oxide surface. For practical reasons, the detection limits of the experiment are used to identify a site as either one or more types of metal centers whose equilibrium constants and enthalpies of base binding are the same. The XPS spectrum of the dried 5 wt.% PdO/C sample showed two palladium peaks at 336.8 ( $3d_{5/2}$ ) and 342.1 eV ( $3d_{3/2}$ ). The non-Gaussian nature of the peaks suggested that both Pd(0) and Pd(II) were presented, thus the representation PdO/C reflects this mixture. In addition, the calorimetric and adsorption results presented the same saturation adsorption capacity for site one, whereas its magnitude proposes that the adsorbed pyridine is normal to the surface plane of PdO. This adsorption process involves a Lewis acid-base type of interaction. Analyzing the low-coverage region, the adsorption quotients of the base onto palladium oxide are considerably larger than those of carbon, which represents preferential adsorption of the base onto the palladium oxide surface, despite the high adsorbing power of the carbon support. The thermodynamic data for

pyridine interaction are:  $-\Delta H_1 = 54.4 \text{ kJ mol}^{-1}$ ;  $n_1 = 2.5 \text{ mmol g}^{-1}$ ;  $-\Delta H_2 = 41.8 \text{ kJ mol}^{-1}$ ;  $n_2 = 3.2 \text{ mmol g}^{-1}$ . It was claimed that the Cal-Ad method using the multiple processes approach provided more resolution of the two sites and the binding enthalpies than TGA or DSC measurements for this catalyst and could be used for other catalysts.

In another research report, Chronister et al. [89] studied silica gel under various hydration conditions by the Cal-Ad method using pyridine as a donor probe. Silica gel is an amorphous material derived from  $\text{SiO}_2$  having a highly porous form. This solid has great importance because it is used as a support in heterogeneous catalysis, as well as separations, microelectronic fabrication, and bioactive bioglass products [96–98]. In addition, silica has been widely studied by many spectroscopy methods (e.g., infrared spectroscopy, and nuclear magnetic resonance). The Cal-Ad method proved to be more sensitive than other characterization techniques for finding three hydrogen bonding sites of different strengths (Figure 4). In previous studies, it was considered that the silica surface was formed by only one type of hydrogen-bonding site [99,100]. Previous studies based on models of silsesquioxanes showed that sites of differing reactivity were expected to be present on the surface, which depended on the extension of hydrogen bonding between neighboring hydroxyls. Accordingly, isolated silanols are less acidic than clusters taking at least three commonly hydrogen-bonded hydroxyl groups [101]. Thus, the Cal-Ad method was able to obtain the enthalpy and equilibrium constant of binding, and the number of each of these sites (e.g., for silica evacuated at  $28 \text{ }^\circ\text{C}$ :  $-\Delta H_1 = 52.7 \text{ kJ mol}^{-1}$ ;  $n_1 = 0.86 \text{ mmol g}^{-1}$ ;  $-\Delta H_2 = 22.2 \text{ kJ mol}^{-1}$ ;  $n_2 = 0.86 \text{ mmol g}^{-1}$ ).

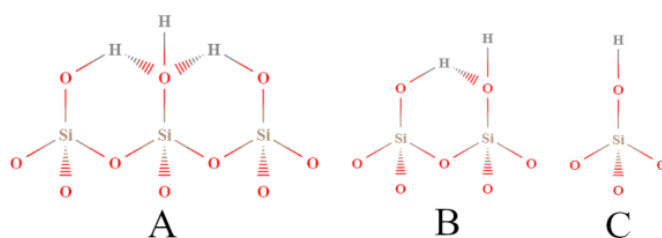


**Figure 4.** Types of silanol sites distinguished by the Cal-Ad method: (A) bridged; (B) vicinal; (C) isolated (terminal). Adapted from reference [89]. Copyright © 1993 ACS.

Hino et al. [102] reported for the first time that zirconium oxide modified with sulfate on the surface develops as a strong solid acid with unique acid catalytic activity. Then, many research papers reported on their catalytic activity. Since these catalysts can perform low-temperature hydrocarbon isomerizations, it has been attributed to sulfated zirconia (SZ) and metal-doped sulfated zirconia superacidity or at least very strong solid acids. Thus, Drago et al. [92] used the Cal-Ad method with pyridine as a probe to determine the acidity of sulfated zirconia and metal-doped sulfated zirconia. Two types of acid sites were detected: the strongest showed  $-\Delta H_1 = 130.5 \text{ kJ mol}^{-1}$  with  $n_1 = 0.027 \text{ mmol g}^{-1}$ ; whereas the other showed  $-\Delta H_2 = 107.9 \text{ kJ mol}^{-1}$  and  $n_2 = 0.055 \text{ mmol g}^{-1}$ . Compared to other strong solid acids also measured by Cal-Ad, SZ acidity ( $-\Delta H_1$ ) is lower than that of HZSM-5 ( $176.2 \text{ kJ mol}^{-1}$ ) or HY ( $142.6 \text{ kJ mol}^{-1}$ ). Doping sulfated zirconia with 0.2 wt.% Pt keeps the same acidity, but doping with Fe and Mn decreases its acidity ( $108.8 \text{ kJ mol}^{-1}$ ). Practically none of the strongest acid sites for SZ remained in the Fe-Mn-SZ, which suggested that both metals were deposited onto those acid sites. Reactions of the SZ sample activated at  $600 \text{ }^\circ\text{C}$  in the pentane isomerization at  $50 \text{ }^\circ\text{C}$  showed 33% conversion of pentane after 30 h, which agrees with other reports on the activity of SZ on light paraffin isomerization. Nonetheless, the SZ superacidity was discussed based on the acidity and the activity for the alkylation of isobutane with 2-butene.

Kob et al. [93] described the preparation of a tungsten (VI) oxide onto silica gel using a precursor of  $\text{WCl}_6$  (SG-W) with excellent dispersion (97%) of the active phase, according to XPS calculation. This is compared to the conventional preparation (impregnation of tungstic acid on silica surface), which showed only 67% dispersion. The

general characterization also included FT-IR, Raman, XRD, BET analysis, and SEM images. After calcination at 200 °C, the characterization indicated that the anchoring unit is  $(\text{SGO})_{4-n}\text{-W}(\text{OH})(\text{O}-)_{1+n}$ , which is attached to octahedral  $\text{WO}_3 \cdot \text{H}_2\text{O}$  aggregates. The Cal-Ad method was conducted on the SG-W catalyst and SG- $\text{WO}_3$  catalysts with the following results for SG-W:  $-\Delta H_1 = 132.6 \text{ kJ mol}^{-1}$ ;  $n_1 = 0.065 \text{ mmol g}^{-1}$ ;  $\Delta H_2 = 67.8 \text{ kJ mol}^{-1}$ ; and  $n_2 = 0.41 \text{ mmol g}^{-1}$ . The strength of the sites was considered comparable within the experimental error, but clearly the number of acidic sites on SG material was superior to SG- $\text{WO}_3$ . Moreover, there was a good correlation between Cal-Ad and XPS data. The characterization shows that SG-W is a Brønsted acid with  $(\text{SiO})_n\text{WOH}$  acceptor sites. The representation of the surface species is  $(\text{SiO})_{4-n}\text{W}(\text{OH})(\text{O}-)_{1+n}(\text{WO}_3 \cdot x\text{H}_2\text{O})_{5.5}$ . Moreover, a short comparison with pure  $\text{WO}_3$  and  $\text{H}_2\text{WO}_4$  (tungstic acid) showed that the strongest sites of both SG-W and SG- $\text{WO}_3$  are stronger than these tungsten compounds. Then, the SG-W catalyst was tested in the alkylation of phenol with methanol, which is considered a model reaction for evaluating the acidity of solid acids [103,104], forming anisole and cresols as the primary reaction products.

Xu et al. [94] studied multinuclear ( $^1\text{H}$ ,  $^{13}\text{C}$ ,  $^{27}\text{Al}$ ,  $^{15}\text{N}$ ,  $^{31}\text{P}$ ) MAS NMR, calorimetry and density functional theory (DFT), providing a consistent interpretation of the acidity of the solid acid catalyst of aluminum chloride supported on silica gel ( $(\text{SG})_n\text{AlCl}_2$ ). The preparation of this solid acid is specifically important to reach maximum strength. It involves the activation of silica gel in a specific way, followed by a reaction with  $\text{Al}_2\text{Cl}_6$  under refluxing with  $\text{CCl}_4$  [94,105]. The results of those studies determined that the acid sites are Brønsted in nature with strength significantly higher than that observed in zeolites. The total number of acid sites was determined by MAS  $^1\text{H}$  NMR as  $0.58 \text{ mmol g}^{-1}$ . By calorimetry using pyridine as a probe molecule,  $0.03 \text{ mmol g}^{-1}$  with  $-\Delta H_1 = 217.6 \text{ kJ mol}^{-1}$  was obtained, and a second site with about  $0.1 \text{ mmol g}^{-1}$  with  $-\Delta H_2 = 184.1 \text{ kJ mol}^{-1}$ . A possible third site could be detected by calorimetry, but the full Cal-Ad method could not be applied in this system because of experimental limitations. Local DFT calculations at the SVWN/DZVP2 level were used to predict the structure and energetics of this catalyst, leading to a conclusion of acid sites stronger than in zeolites. Thus, with all these data from the above techniques,  $(\text{SG})_n\text{AlCl}_2$  was considered as a catalyst with a Brønsted acid strength on the threshold of superacidity.

#### 4.2. Zeolites

Most chemical reactions involving heterogeneous catalysis deal with the adsorption of a liquid or gas on the surface of the catalyst. The correlation of reactivity to acidity is essential since different acid site strengths are required according to acid-catalyzed reactions. In order to characterize the catalyst and its reaction mechanisms, solid surface microcalorimetry methods have been shown to be an important tool, since they can be coupled to other spectroscopic techniques. Among the solid acids for which the thermodynamic parameters were determined by the Cal-Ad method, zeolites play a prominent role due to their microporous crystalline structures. Then, Drago et al. [90] studied HZSM-5 ( $\text{Si}/\text{Al} = 36$ ) acidity using three different bases (pyridine, 2,6-lutidine, and 2,6-di-tert-butylpyridine), and two types of sites were resolved indicating that both sites react simultaneously even at lower base concentration. The Cal-Ad isotherms for pyridine adsorption are shown in Figure 5. Pyridine was chosen as the donor to avoid the amphoteric interaction observed when protonic donors (e.g.,  $\text{NH}_3$ ) are used, promoting an increased hydrogen bonding of the N-H proton to the framework. Comparison of the pyridine enthalpy interaction indicated a stronger Brønsted site ( $-\Delta H_1 = 176.1 \text{ kJ mol}^{-1}$ ) than silica gel and  $\gamma$ -alumina, but not superacid as aluminum chloride supported on silica gel ( $(\text{SG})_n\text{AlCl}_2$ ) [94]. The thermodynamic data for the second site on HZSM-5 ( $-\Delta H_2 = 35.9 \text{ kJ mol}^{-1}$ ) is comparable to that of the sites on silica gel. In relation to the other two bases, 2,6-di-tert-butylpyridine cannot enter the channels and provides information about the acidity of the external solid surface (i.e.,  $-\Delta H_1 = 45.6 \text{ kJ mol}^{-1}$ ) indicating the strongest sites are in the channels. Using 2,6-lutidine, the highest enthalpy ( $-\Delta H_1 = 79.5 \text{ kJ mol}^{-1}$ ) suggests that there is an average

between some strong sites with others that are weaker, but both are hydrogen bonding type sites. A detailed analysis of all data ( $-\Delta H_1$ 's and  $n$ 's) indicated up to four site types: a strong, but limited access (I); limited access hydrogen bonding (II); interior hydrogen bonding (III); and surface (IV). The fair agreement between the  $0.6 \text{ mmol g}^{-1}$  sites found by Cal-Ad and the  $0.5 \text{ mmol g}^{-1}$  sites found in the gas phase of a similar HZSM-5 sample suggests that pyridine migrates from site to site during the few second time scale of the solution calorimetry ( $25^\circ\text{C}$ ).

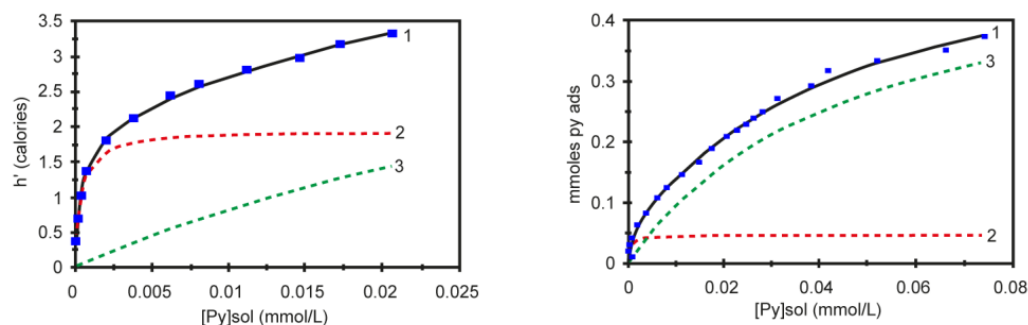


**Figure 5.** Experimental data curve (1) and fitted isotherms to process one (dashed red line) and process two (dashed green line) for two-site model of the calorimetric (left) and adsorption (right) experiments. Adapted from reference [90]. Copyright @ 1997 ACS.

TS-1 is a titanium derivative of silicalite-1 that has a ZSM-5 (MFI) structure with a small fraction of isomorphous framework substitution of  $\text{Si}^{\text{IV}}$  by  $\text{Ti}^{\text{IV}}$  (containing 1 wt.% titanium) [106]. TS-1 was studied by Drago et al. [107] and showed catalytic properties for the epoxidation of propylene using  $\text{H}_2\text{O}_2$ . A comparison of the enthalpy of the interaction of pyridine for the first site of TS-1 with that for HZSM-5 shows that TS-1 does not have the very strong acid sites of HZSM-5 but rather has only silanol hydrogen-bonding sites such as silica gel ( $-\Delta H_1 = 63.2 \text{ kJ mol}^{-1}$ , and  $n_1 = 0.07 \text{ mmol g}^{-1}$ ). Thus, the Cal-Ad results confirmed that TS-1 presents less capacity for water adsorption (less hydrophilic) than HZSM-5 or even silica gel. Cal-Ad provided information about the donor-acceptor interaction and indicated a greatly reduced amount of hydrogen-bonding functionality on the interior and exterior surface of TS-1 compared to that of HZSM-5 or silica gel, without any Brønsted or Lewis strong sites. The determination of the increased dispersion interaction based on the multiple equilibrium analysis (MEA) of gas phase adsorption isotherms of different probes explains the hydrophobic properties of TS-1 compared to HZSM-5. The main utilization of TS-1 in epoxidation can be explained by the absence of strong acid sites, which prevent epoxide ring opening.

Another important zeolite (Y zeolite,  $\text{Si}/\text{Al} = 6.8$ ) was evaluated by Cal-Ad [108], which had its acid strength distribution measured with six different bases: pyridine; 2,6-lutidine; 2,6-di-tert-butylpyridine; quinoline; tetrahydrothiophene; and benzonitrile. The size of the probe molecules plays a fundamental role in the accessibility and hence the determination of acid site distribution on the zeolite. The results indicated the presence of three families of acid sites. The strongest sites ( $-\Delta H_1 > 121 \text{ kJ mol}^{-1}$ ) showed a significant number of Brønsted sites ( $n = 0.1 \text{ mmol g}^{-1}$ ) located inside the large cages ( $\sim 1.3 \text{ nm}$ ) or near where probes can have access through the channel of  $0.74 \text{ nm}$  opening. The sites of intermediary strength ( $-\Delta H_1 \sim 71 \text{ kJ mol}^{-1}$ ) are Lewis and Brønsted types located near the external surface and extra-framework species. The weaker sites ( $-\Delta H_1 < 42 \text{ kJ mol}^{-1}$ ) located at the external surface contain significant hydrogen bonding types. The strength of these sites is related to the mutual interaction between Lewis and Brønsted sites. Pyridine and 2,6-lutidine are titrating sites inside the large and on the border of sodalite cages and because of steric effects, the enthalpy for 2,6-lutidine is lower than that for pyridine. On account of the similar amounts ( $n_2 \sim 0.2 \text{ mmol g}^{-1}$ ) and enthalpies ( $-\Delta H_1 \sim 75.3 \text{ kJ mol}^{-1}$ ), the second site for pyridine and 2,6-lutidine along with the first site for 2,6-di-tert-butylpyridine (DTBpy) is located near to the surface of the solid. The low interaction between DTBpy and

the acid sites of Y zeolite sites ( $-\Delta H_1 = 78.7 \text{ kJ mol}^{-1}$ ) is related to the inaccessibility of some sites located at the hexagonal prism and sodalite unit and the size of DTBpy, which limits the number of molecules that can be fitted in the supercavities. In addition, the lower heat may be attributed to the lower pKa value for DTBpy (3.58) in relation to pyridine (5.17). Due to microporosity, thermal energy can be enough for the adsorbed molecules to diffuse along the surface and adsorb preferentially on the strongest sites at low coverages followed by adsorption on weaker ones as the surface coverage increases. Moreover, the application of the electrostatic-covalent model (ECW) to Y zeolite provided quantitative parameters for the determination of donor-acceptor contributions based on electrostatic ( $E_A$ ) and covalent ( $C_A$ ) intrinsic characters to each chemical bonding. The results indicated that zeolite Y has a stronger covalent character with  $E_A = 5.25$ ,  $C_A = 6.89$  ( $C_A/E_A = 1.31$ ) consistent with softness properties proposed in the literature and higher than for silica gel ( $C_A/E_A = 1.08$ ).

Fluid catalytic cracking (FCC) of crude oil distillates uses faujasite-type zeolites (X and Y), and mainly with incorporated rare-earth as a component of the catalyst for this process [109–111]. Thus, knowledge of the acidic properties of each component and the whole catalyst is required. Ghesti et al. [112] prepared a protonic ultrastabilized Y zeolite (USY, Si/Al = 1.3) modified by the insertion of cerium (5 wt.%) and characterized its acidity by Cal-Ad, pyridine gas-phase adsorption/desorption (Py-TPD), and FT-IR. The Cal-Ad method detected a two-site model best fit for both samples: USY ( $-\Delta H_1 = 134.0 \text{ kJ mol}^{-1}$ ;  $n_1 = 0.139 \text{ mmol g}^{-1}$ ;  $-\Delta H_2 = 101.5 \text{ kJ mol}^{-1}$ ;  $n_2 = 0.737 \text{ mmol g}^{-1}$ ), and Ce/HUSY ( $-\Delta H_1 = 117.6 \text{ kJ mol}^{-1}$ ;  $n_1 = 0.062 \text{ mmol g}^{-1}$ ;  $-\Delta H_2 = 83.6 \text{ kJ mol}^{-1}$ ;  $n_2 = 0.791 \text{ mmol g}^{-1}$ ). In HUSY,  $n_1$  and  $n_2$  corresponded to Brønsted sites. After cerium impregnation, the zeolite material showed a significant reduction in stronger acid sites and neutralization of weaker ones. Furthermore, thermodynamic values and DRIFTS results suggested that cerium species interacted just with 47% of the strongest HUSY sites, leading to a reduction of  $n_1$  and a 52% increase in  $n_2$  (weaker Brønsted and Lewis sites). The total number of sites is similar by both Py-TPD and Cal-Ad and indicated that not all Al sites are accessible to pyridine in these materials.

Mordenite zeolite is generally used in hydrocracking, alkylation, dewaxing, separation, and purification reactions [113]. Cal-Ad analysis of HMOR (Si/Al = 6.5) using cyclohexane as the solvent [114] revealed the presence of two predominant sites: the first site ( $n_1 = 0.081 \text{ mmol g}^{-1}$ ) was assigned as Brønsted ( $-\Delta H_1 = 82.9 \text{ kJ mol}^{-1}$ ), while the second site ( $n_2 = 0.422 \text{ mmol g}^{-1}$ ) can be assigned as Lewis ( $-\Delta H_2 = 36.7 \text{ kJ mol}^{-1}$ ). A comparison between the total number of sites found by Cal-Ad ( $n_T = 0.50 \text{ mmol g}^{-1}$ ) to the total Al atoms on the sample ( $n_T = 0.89 \text{ mmol g}^{-1}$ ) shows that 56% of the accessible sites are in the main channels and 44% in the side pockets of mordenite. The FT-IR spectrum of the HMOR shows that the adsorption of pyridine gives rise to the appearance of bands related to the Brønsted (1547 and 1491  $\text{cm}^{-1}$ ) and Lewis (1491 and 1452  $\text{cm}^{-1}$ ) sites, which are compatible with Cal-Ad results.

One more zeolite was chosen for acidity evaluation by the Cal-Ad method. \*BEA zeolite presents a truncated bipyramidal shape with relatively voluminous channels, allowing it to carry out several acid and redox catalyzed reactions within its inner volume [115]. This zeolite (Si/Al = 12.5) had its acidity adjusted for two and three sites [116]. Adjustment for three sites in a sample treated at 450 °C indicated a very small amount of very strong sites. However, the \*BEA treated at 550 °C, according to studies in the literature [117] and recent results from our laboratory [118,119], showed a good adjustment for two sites ( $-\Delta H_1 = 148 \text{ kJ mol}^{-1}$ ;  $n_1 = 0.15 \text{ mmol g}^{-1}$ ;  $-\Delta H_2 = 61.8 \text{ kJ mol}^{-1}$ ;  $n_2 = 0.40 \text{ mmol g}^{-1}$ ). The \*BEA zeolite after adsorption of pyridine showed an FT-IR spectrum with both Brønsted and Lewis sites in agreement with the Cal-Ad.

#### 4.3. Heteropolyacids and Derivatives

Dias et al. [120] studied the heteropolyacid (HPA) 12-tugstophosphoric acid ( $\text{H}_3\text{PW}_{12}\text{O}_{40}$ , HPW), which is considered the strongest Keggin HPA. This work aimed to measure the

acidity of HPW using the Cal-Ad method with pyridine as a probe molecule. The analysis showed that the protons of the solid HPW have different strengths. The method could detect two distinct types of acidic protons (sites) with populations ( $n$ ) and enthalpies ( $\Delta H$ ) of interaction with pyridine in a cyclohexane slurry with the following components:  $-\Delta H_1 = 136.8 \text{ kJ mol}^{-1}$ ;  $n_1 = 0.08 \text{ mmol g}^{-1}$ ;  $-\Delta H_2 = 82.0 \text{ kJ mol}^{-1}$ ;  $n_2 = 0.16 \text{ mmol g}^{-1}$ . The total number of protons titrated ( $0.24 \text{ mmol g}^{-1}$ ) verified that not all of the available protons of HPW ( $1.04 \text{ mmol g}^{-1}$ ) reacted with pyridine. A structural analysis (Figure 6) suggested that this total could be assigned to the number of protons in every even plane of the lattice (E00). The different protons can be ascribed to the face ( $n_1$ ) and edge ( $n_2$ ) positions in the cubic unit cell of HPW. The total number of protons of HPW titrated with pyridine ( $0.24 \text{ mmol g}^{-1}$ ) was higher than the number of calculated surface protons ( $0.008 \text{ mmol g}^{-1}$ ), which confirmed, one more time, that polar molecules can react in the bulk of the crystal as well as on the surface. This behavior is analogous to that of a concentrated solution and is explained as a pseudoliquid phase, i.e., polar molecules such as pyridine can be adsorbed in the bulk but not nonpolar molecules [121,122]. The spectroscopic techniques (FT-IR and  $^{31}\text{P}$  MAS NMR) and XRD were used to characterize the HPW and their adducts with Py adsorbed. The FT-IR spectra confirmed the characteristic Keggin bands and the formation of pyridinium ion through the presence of very characteristic bands at  $1540$  and  $1485 \text{ cm}^{-1}$ , which are attributed to Brønsted sites, as usually ascribed in different solid acids [57]. XRD results confirmed structure opening as pyridine is absorbed in sites one and two by the increase in the cell parameter. Proton mobility was observed using  $^{31}\text{P}$  MAS NMR spectra of HPW-pyridine adducts showing unique signals for different HPW to pyridine ratios. Drago et al. [95] studied the acidity of HPW in  $\text{CH}_3\text{CN}$  solution and calculated its  $C_A/E_A$  ratio of 2.88, which indicates significant covalency in the interactions of HPW acceptors. In addition, the solvation enthalpy of acetonitrile to HPW (i.e.,  $\text{HPW} + 3\text{CH}_3\text{CN} \rightarrow (\text{CH}_3\text{CN})_3\text{HPW}$ ) was obtained as  $-40.6 \text{ kJ mol}^{-1}$ . This value added to the binding enthalpy of pyridine in  $\text{CH}_3\text{CN}$  ( $\Delta H = -87.9 \text{ kJ mol}^{-1}$ ) leading to an enthalpy of  $-128.5 \text{ kJ mol}^{-1}$ , which is in fair agreement with the Cal-Ad measurement of the strongest site of HPW ( $-\Delta H_1 = 136.8 \text{ kJ mol}^{-1}$ ).

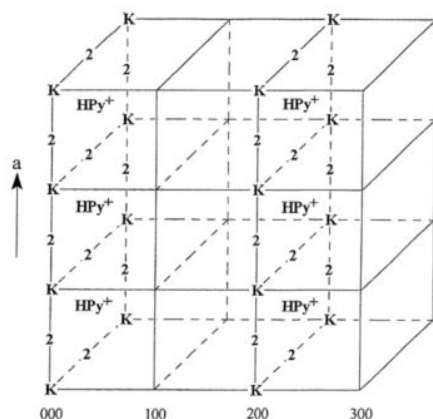


**Figure 6.** Cubic structure of HPW–pyridine adduct with site one completely titrated, showing only the Keggin anion (K) and protonated pyridine (HPy<sup>+</sup>) of the even planes for clarity. The face-centered protons of every even plane (E00) have reacted with an incoming pyridine molecule to form pyridinium and the site two protons are represented by the number two. Adapted from reference [120]. Copyright © 1999 Elsevier, License Number: 5517660705294.

The acidity of HPW was further probed by dehydration of 1-propanol in research by Dias et al. [123]. The activation of  $\text{H}_3\text{PW}_{12}\text{O}_{40}$  under different thermal conditions has been evaluated by calorimetry and correlated to the conversion of 1-propanol. It was demonstrated that thermal treatments at 200, 300, and 400 °C have substantial changes in the catalytic activity of HPW as a function of temperature and time of activation. The correlation of the calculated enthalpies and the percent conversion (Figure 7) of 1-propanol

is linear ( $r^2 = 0.991$ ), and activation energies for the dehydration are about 71 to 75  $\text{kJ mol}^{-1}$ , which are in the range for other solid acids for the same process and consistent with no diffusional constraints.

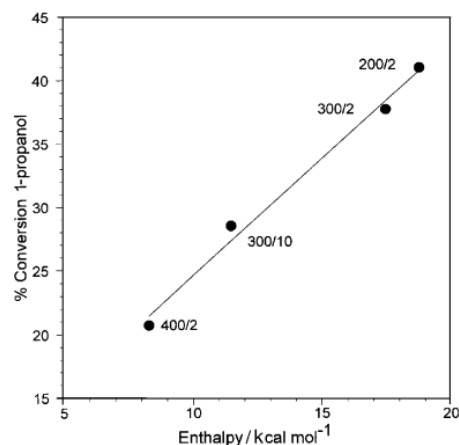


**Figure 7.** Conversion of 1-propanol catalyzed by HPW, calcined at different temperatures ( $^{\circ}\text{C}$ )/times (h). Adapted from reference [123]. Copyright © 2001 RSC, License Number: 5512345678910.

Dias et al. [124] studied cesium salts of 12-tungstophosphoric acid (HPW), i.e., with formulas  $\text{Cs}_x\text{H}_{3-x}\text{PW}_{12}\text{O}_{40}$  (abbreviated as  $\text{Cs}_x\text{H}_{3-x}\text{PW}$ ) because of their notorious and commented superacidity, shape selectivity, and hydrophobicity [125]. However, unlike HPW,  $\text{Cs}_x\text{H}_{3-x}\text{PW}$  salts have very limited solubility in water or organic solvents and are used exclusively as heterogeneous catalysts. While cesium derivatives show greater thermal stability, some of them have greater catalytic activity in certain reactions than HPW [126–128]. Salts in the  $\text{Cs}_x\text{H}_{3-x}\text{PW}_{12}\text{O}_{40}$  series ( $x = 1; 2; 2.5; \text{ and } 3$ ) are prepared and characterized by structure and acidity using the Cal-Ad method. XRD, FT-IR, and  $^{31}\text{P}$  MAS NMR confirmed the formation of salts, whereas microcalorimetry is capable of distinguishing the strength and quantity of the different acid sites in the catalysts. The distribution of protons and cesium ions in the salt structures is almost homogeneous according to stoichiometry, confirmed by XRD and  $^{31}\text{P}$  MAS NMR. Furthermore, Cal-Ad enthalpy measurements indicate that no mechanical mixing of the salts is produced under these experimental conditions, confirming the description of these salts as solid solutions. The Cal-Ad results indicate the protons distributed in these solids have different strengths, leading to the following order of acidity:  $\text{HPW} > \text{Cs}_2\text{HPW} \geq \text{Cs}_{2.5}\text{H}_{0.5}\text{PW} > \text{CsH}_2\text{PW} > \text{Cs}_3\text{PW}$ , with enthalpies of  $-\Delta H_1 = 136.8; 117.9; 114.6; 87.0; \text{ and } 32.6 \text{ kJ mol}^{-1}$ , respectively. These enthalpies are influenced by an endothermic term related to the interstitial expansion of the lattice by the addition of the pyridine molecule, which is evidenced by XRD results. The nature of the sites in these  $\text{Cs}_x\text{H}_{3-x}\text{PW}_{12}\text{O}_{40}$  series was Brønsted and hydrogen bonding, according to FT-IR of pyridine adsorption.

Many properties of HPA can be improved by preparing supported materials. For instance, enhancement of the specific surface area, development of higher dispersion of acidic protons, heterogenization of homogeneous systems, and fine control of acid strength. Thus, different matrices (e.g., silica, alumina, zirconia, silica-alumina, carbon) can be used for that goal [129,130]. The potentiality of these supported HPAs can be illustrated in many examples.

One of the most commonly supported HPA uses silica as a matrix. Dias et al. [131] and other researchers [132–137] have pointed to HPA as versatile green catalysts for a variety of reactions (e.g., alkylation and acylation of aromatics, esterification, liquid biphasic processes). Supported HPW samples (8 to 25 wt.%) were prepared and structurally analyzed by FT-IR and XRD to confirm the presence of the Keggin structure. Keggin bands are more evident for samples with HPW contents above 20 wt.%. Using XRD, samples above 8% indicate the existence of HPW nanocrystals by the presence of their characteristic peaks,

but much wider. For mechanical mixtures (HPW + SiO<sub>2</sub>) in different proportions, the FT-IR spectra show the Keggin bands, and by XRD the HPW peaks are shown to be similar to their pure crystalline form. Therefore, great care must be used to characterize supported HPA by these techniques only, in order to differentiate both forms. Calorimetric titrations with pyridine in cyclohexane and the application of the Cal-Ad method were performed on x% HPW/SiO<sub>2</sub> (x ≈ 8 to 25 wt.%) The results of the average enthalpies (calculated based on the limiting reagent assumption) show that the interaction of HPW with SiO<sub>2</sub> is relatively strong ( $-\Delta H_{1(AVG)} = 108.8 \text{ kJ mol}^{-1}$ ), comparatively to pure SiO<sub>2</sub> ( $-\Delta H_1 = 52.7 \text{ kJ mol}^{-1}$ ) for the strongest site, and almost independent of the HPA content from 15 to 25 wt.%. However, these catalysts are weaker than pure HPW. The lower the HPW content in the silica, the lower the enthalpies, indicating that a stronger interaction will occur with the silica surface, leveling the stronger acidic solid sites with the weaker ones. The strength of the acidic sites of the 25% HPW/SiO<sub>2</sub> sample shows enthalpies of  $-\Delta H_1 = 116.7 \text{ kJ mol}^{-1}$  and  $-\Delta H_2 = 42.3 \text{ kJ mol}^{-1}$  which are lower than the free acid (e.g.,  $-\Delta H_1 = 136.8 \text{ kJ mol}^{-1}$  and  $-\Delta H_2 = 82.0 \text{ kJ mol}^{-1}$ ). However, the greater dispersion and larger accessibility of the stronger sites are demonstrated (e.g.,  $n_T = 0.102 \text{ mmol g}^{-1}$  versus  $0.08 \text{ mmol g}^{-1}$  for HPW). The nature of HPW/SiO<sub>2</sub> sites obtained by FT-IR and confirmed by Cal-Ad reveals pyridinium ion bands for the strongest site (Brønsted) and hydrogen-bonded pyridine to the weakest. Furthermore, the acidic order is consistent with the literature results by other methods (e.g., microcalorimetry of NH<sub>3</sub> adsorption) where pure HPW is stronger than supported HPW/SiO<sub>2</sub>.

After this full characterization of x% HPW/SiO<sub>2</sub> catalysts, they were applied in benzene transalkylation with C<sub>9+</sub> aromatics, using an industrial stream by Dias et al. [138]. Aromatic compounds are important raw materials for intermediates of petrochemicals and fine chemicals (e.g., benzene, toluene, and xylenes—BTX). The reforming and gasoline pyrolysis are major industrial suppliers of BTX and produce noticeable contents of trimethylbenzene and toluene. Then, a suitable way to upgrade the low value C<sub>7</sub> and C<sub>9</sub> aromatics is to convert them to benzene and xylenes. Due to environmental issues with the use of benzene, its transformation by transalkylation with C<sub>9+</sub> aromatics is a significant reaction for commercial applications [139]. Thus, using x% HPW/SiO<sub>2</sub> catalysts (x = 8, 15, 20 and 25 wt.%), the activity and selectivity to xylenes vary with the acid loading, and this is related to optimum acid strength, dispersion, and specific surface area of the solid acids. The most active catalyst was the 15 wt.% HPW, which revealed a satisfactory combination of the three cited properties (Table 1). The 15% HPW/SiO<sub>2</sub> catalyst is the most stable in the series and underwent the lowest rate of deactivation, forming the lowest amount of coke under the reaction conditions. Compared to the commercial catalyst of zeolite mordenite, it presented the highest activity and selectivity to xylenes, which showed a promising profile for industrial applications of this type of catalyst.

**Table 1.** Physical-chemical properties, acidity ( $-\Delta H$  and  $n_T$ ), selectivity to xylene (xy), and coke (spent catalyst) of the transalkylation reaction of trimethylbenzene with benzene using x% H<sub>3</sub>PW/SiO<sub>2</sub>. Adapted from reference [138]. Copyright © 2007 Elsevier, License Number: 5517670709148.

Catalyst (%H <sub>3</sub> PW)	S <sub>BET</sub> <sup>a</sup> (m <sup>2</sup> g <sup>-1</sup> )	S <sub>BET</sub> <sup>b</sup> (m <sup>2</sup> g <sup>-1</sup> )	D <sub>XRD</sub> <sup>c</sup> (nm)	$-\Delta H_{AVG}$ (kJ mol <sup>-1</sup> )	$n_T$ (mmol g <sup>-1</sup> )	Sel <sub>(XY)</sub> (%)	Coke (%)
8	74	23	12	85.9	0.078	0	1.6
15	63	60	15	100.4	0.159	3.9	0.3
20	57	43	17	108.8	0.204	2.8	1.0
25	40	20	18	116.7	0.252	0	2.4
MOR	n.a.	n.a.	n.a.	82.9	0.503	2.1	14.1

<sup>a</sup> Specific surface area of fresh catalysts. <sup>b</sup> Specific surface area of spent catalyst. <sup>c</sup> Crystallite domain sizes (Scherrer equation) from XRD patterns of the fresh catalyst (HPW 2 $\theta$  = 10.28, plane (1 1 0)).

Alumina is an often-used support for various catalysts in the literature. Some older reports indicate the decomposition of HPA supported on Al<sub>2</sub>O<sub>3</sub>. Thus, Caliman et al. [140]

using the Cal-Ad method, besides structural characterization, prompted us to study in detail  $x\%$  HPW/ $\text{Al}_2\text{O}_3$  ( $x = 20, 40, 50,$  and  $80$  wt.%) using  $\gamma$ -alumina. Impregnation of HPW on  $\gamma$ -alumina was carried out in solution, followed by evaporation using water (acidified with HCl), ethanol, and acetonitrile as solvents. The presence of the intact Keggin anion on  $\gamma$ -alumina surface is extremely dependent on the solvent, the preparation conditions, and pH when using an aqueous phase. Thus, an acid concentration of at least  $0.1 \text{ mol L}^{-1}$  should be used when evaporation of the solvent is employed as a technique. These conclusions could be achieved based on XRD, FT-IR, FT-Raman,  $^{31}\text{P}$  MAS NMR, and SEM-EDX measurements. In addition, the Cal-Ad method using pyridine proves that the strongest sites of the catalyst  $20\%$  HPW/ $\text{Al}_2\text{O}_3$  ( $-\Delta H_1 = 94.6 \text{ kJ mol}^{-1}$ ) is a weaker acid than pure HPW ( $-\Delta H_1 = 136.8 \text{ kJ mol}^{-1}$ ) or  $25\%$  HPW/ $\text{SiO}_2$  ( $-\Delta H_1 = 116.7 \text{ kJ mol}^{-1}$ ), but it is stronger than  $\gamma$ -alumina ( $-\Delta H_1 = 63.6 \text{ kJ mol}^{-1}$ ). These enthalpies clearly indicate partial neutralization of the most basic sites of  $\gamma$ -alumina at the expense of the strongest protons of HPW. Moreover, compared to pure HPW ( $n_1 = 0.08 \text{ mmol g}^{-1}$ ), the protons on  $20\%$  HPW/ $\text{Al}_2\text{O}_3$  ( $n_1 = 0.154 \text{ mmol g}^{-1}$ ) are much more accessible. Therefore, more protonic sites are available for surface-type catalytic reactions, even though the strength is much lower than pure or supported HPW on silica. The Cal-Ad model fits a two-site system, which is supported by the FT-IR spectra of the adsorbed pyridine. The FT-IR absorption region of pyridine adducts showed bands relative to Brønsted and Lewis sites.

Caliman et al. [141] prepared catalysts of  $x\%$  HPW/ $\text{Nb}_2\text{O}_5$  with a wide range of loadings ( $20$ – $60$  wt.%) by impregnation in aqueous acid solution (HCl,  $0.1 \text{ mol L}^{-1}$ ) and characterized by XRD, FT-IR, FT-Raman,  $^{31}\text{P}$  MAS NMR, adsorption of  $\text{N}_2$  at low temperature ( $-196 \text{ }^\circ\text{C}$ ), and pyridine adsorption/desorption in the gas phase. In addition, the acidity was measured by the Cal-Ad method using pyridine, and a two-site model gave for  $25\%$  HPW/ $\text{Nb}_2\text{O}_5$ :  $-\Delta H_1 = 119.7 \text{ kJ mol}^{-1}$ ;  $n_1 = 0.086 \text{ mmol g}^{-1}$ ;  $-\Delta H_2 = 43.5 \text{ kJ mol}^{-1}$ ;  $n_2 = 0.191 \text{ mmol g}^{-1}$ . It is important to note that about  $33\%$  of the total protons were accessible for  $25\%$  HPW/ $\text{Nb}_2\text{O}_5$ , whereas only  $8\%$  was obtained for pure HPW. Using FT-IR to study pyridine adsorbed on these catalysts, two sites were also observed: pyridinium ion (Brønsted type sites) and probably hydrogen bonding sites, since no Lewis sites were detected, which agrees with the Cal-Ad measurements. It is worth noting that the accessibility of the pyridine probe to the strongest acid sites is facilitated by the dispersion of HPW on the niobium surface, as well as other studied supports. The order of accessibility based on  $n_1$  values of various supported HPW is  $\text{HPW}/\text{Al}_2\text{O}_3 > \text{HPW}/\text{SiO}_2 > \text{HPW}/\text{Nb}_2\text{O}_5 > \text{HPW}$ . Therefore, supporting HPA on different matrices can control important parameters of solid acidities, such as the strength and quantity of surface acid sites on this class of catalysts.

Activated carbon is another support that entraps HPA in pores forming insoluble compounds that do not leach the polyacid. The catalyst is used for liquid-solid and gas-solid organic reactions even in polar media. Characterization of HPW/carbon (HPW/C) performed by microcalorimetry with  $\text{NH}_3$  adsorption [142] indicates that the interaction of HPW with activated carbon is strong. In this sense, Chafran et al. [143] prepared  $x\%$  HPW/C catalysts ( $x = 20, 30, 40,$  and  $50$  wt.%) by impregnation/evaporation solution of HPW on activated carbon (Norbit<sup>®</sup> SA3). The catalysts were characterized and further applied to the polymerization of D,L-lactic acid forming blends of poly(lactic acid) (PLA). Thermal treatments between  $200$  and  $500 \text{ }^\circ\text{C}$  tested the stability of the Keggin anion, and the results indicated that calcination should not be beyond  $400 \text{ }^\circ\text{C}$ , based on XRD, FT-IR,  $^{31}\text{P}$  MAS NMR, and textural analyses. It is proposed that proton transfer occurs from the HPW to the basic groups (e.g., hydroxyl groups, lactone) on the carbon surface. Preliminary calorimetric results for the  $20\%$  HPW/C calcined at  $200, 300,$  and  $400 \text{ }^\circ\text{C}$  indicated similar enthalpies, with an average enthalpy of interaction with pyridine ( $-\Delta H_1$ ) of  $95 \text{ kJ mol}^{-1}$ , and the number of the active sites ( $n_1$ ) is  $0.13 \text{ mmol g}^{-1}$  for the strongest sites in this range of calcination. Based on the decomposition temperature ( $T_d$ ), which is the temperature where the polymer decomposes,  $T_d$  was monitored using TG/DTG (thermogravimetry/derivative thermogravimetry). Then, it was possible to evaluate the catalyst performance to produce a more thermally stable material, i.e., with a higher  $T_d$ . Thus,  $20\%$  HPW/C calcined at  $400 \text{ }^\circ\text{C}$

gave the best result for PLA production. It should be mentioned that optimal experimental conditions were achieved to produce PLA forming blends (PLLA and PDLA) with a high level of enantiomeric excess (85%) for PLLA using the former catalyst under the following conditions: 0.1 wt.% catalyst relative to the initial mass of D,L-lactic acid; a temperature of 180 °C; and a 15-h reaction period. Additionally, the 20% HPW/C calcined at 400 °C catalyst was tested in three reutilizations and exhibits high activity (about 95% recovery).

Based on the promising results of PLA production by heterogeneous catalytic synthesis using HPW/C, Chafran et al. [144] used the former optimum conditions to comparatively study HPW supported on silica, alumina, and activated carbon. As it is very widespread in the literature [145], PLA polymer is based on renewable resources and could be used in sustainable plastics. It is a promising biopolymer due to its properties and projected commercial expenses. A recent review by de França et al. [146] indicated a way to enhance the production of PLA including materials that are generated using cheaper sources of monomers such as D,L-lactic acid. In this sense, that work [146] sought to find cheaper supports for HPW (silica and alumina) that under similar conditions of the polycondensation produces PLA with a similarly high level of enantioselectivity. The catalyst 20% HPW/C was studied by the Cal-Ad method since the other supported HPW catalysts (silica and alumina) have been characterized [131,140]. The results ( $-\Delta H_1 = 93.7 \text{ kJ mol}^{-1}$ ;  $n_1 = 0.13 \text{ mmol g}^{-1}$ ;  $-\Delta H_2 = 29.3 \text{ kJ mol}^{-1}$ ;  $n_2 = 0.22 \text{ mmol g}^{-1}$ ) confirmed that HPW supported on silica or alumina has stronger acid sites than the carbon catalysts. The acidity of the catalysts (20 wt.%, calcined at 400 °C) was correlated with the molar mass ( $M_w$ ) of the PLA obtained, which showed the trending  $\text{PLA}(M_w)_{\text{HPW/C}} > \text{PLA}(M_w)_{\text{HPW/Al}_2\text{O}_3} > \text{PLA}(M_w)_{\text{HPW/SiO}_2}$ , whereas the acidity ( $-\Delta H$ ) order was  $\text{HPW/SiO}_2 > \text{HPW/Al}_2\text{O}_3 > \text{HPW/C}$ . The main properties of the catalysts and correlations with some properties of the produced PLA are illustrated in Table 2. Thus, adequate strength and accessibility of their sites is a necessary combination to achieve a successful polycondensation reaction of D,L-lactic acid to produce PLA.

**Table 2.** Properties of the catalysts and correlations with some properties of the produced PLA. Adapted from reference [144]. Copyright © 2019 Elsevier, License Number: 5517671063190.

#	Sample/Polymer	Property (Catalyst) <sup>a</sup>			Property (PLA) <sup>b</sup>		
		$-\Delta H_1$	$n_1$	$n_T$	ee	$M_n$	$M_w$
1	D,L-lactic acid	-	-	-	3	-	-
2	PLA (pre-polymer)	-	-	-	70	2278	2705
3	PLA (no catalyst)	-	-	-	88	4864	7408
4	Carbon	6	-	-	93	4893	9672
5	SiO <sub>2</sub>	53	0.86	1.72	94	5285	8350
6	Al <sub>2</sub> O <sub>3</sub>	64	0.16	0.41	84	5267	7709
7	H <sub>3</sub> PW	130	0.08	0.23	79	5914	9818
8	20% H <sub>3</sub> PW/C	91	0.12	0.34	85	8469	15,189
9	20% H <sub>3</sub> PW/Al <sub>2</sub> O <sub>3</sub>	97	0.12	0.35	95	8161	14,827
10	20% H <sub>3</sub> PW/SiO <sub>2</sub>	110	0.09	0.40	83	7982	14,273

<sup>a</sup>  $-\Delta H_1$  (kJ·mol<sup>-1</sup>) and  $n_1$  (mmol·g<sup>-1</sup>) are for the strongest sites;  $n_T$  ( $n_1 + n_2$ , mmol·g<sup>-1</sup>) is the total acid sites obtained by the Cal-Ad method based on a pyridine probe. <sup>b</sup> PLA properties (ee, enantiomeric excess and the average molar masses,  $M_n$ , and  $M_w$ ) obtained from the respective process with or without catalysts. - data not available.

Freitas et al. [147] synthesized a series of HPA catalysts (H<sub>3</sub>PW<sub>12</sub>O<sub>40</sub> and H<sub>4</sub>SiW<sub>12</sub>O<sub>40</sub>, HPW and HSiW, respectively) supported on zeolite Y, with loadings from 14 to 58 wt.%, via incipient and aqueous impregnation. The acidity of the synthesized catalysts was evaluated by applying two main techniques: gaseous adsorption of pyridine with subsequent FT-IR analysis, and microcalorimetry of pyridine adsorption in cyclohexane of the solids in suspension. The FT-IR spectra with pyridine adsorbed from the x% HPA/Y catalysts showed the disappearance of the band related to Lewis sites present in the HY zeolite and the presence of enhanced Brønsted sites. This was attributed to the interaction

between the Keggin anion and hydroxyl sites on the surface of the support leading the solid to have predominantly Brønsted type sites. The new sites kept the strengths higher ( $-\Delta H = 100 \text{ kJ mol}^{-1}$ ) with a generally increased number ( $n$ ) because the pristine solids have around the same average strength ( $-\Delta H = 147 \text{ kJ mol}^{-1}$ ). Higher conversions for the esterification reaction of butanol and acid acetic to butyl acetate were observed for the samples prepared by incipient impregnation, which is parallel to the higher acidity obtained by these samples by microcalorimetry.

Further, Freitas et al. [148] used the same catalysts ( $x\%$  HPA/Y, where HPA = HPW and HSiW, in proportions of 27 to 44 wt.%) combined with ionic liquids to the Biginelli multicomponent reaction (MCR). Then, a series of experiments were performed involving the optimization conditions (e.g., loading of HPA on zeolite Y, calcination temperature, reaction time) in a model Biginelli reaction (benzaldehyde, urea, and ethyl acetoacetate under equimolar quantities). It was found that higher yields were obtained with supported catalysts that have suitable strength of acid sites ( $-\Delta H = 140 \text{ kJ mol}^{-1}$ ). These catalysts were selected based on the enthalpy data of the acidic sites obtained through microcalorimetry of pyridine adsorption in cyclohexane. This study in the presence and absence of ionic liquids showed that the kinetics of the reaction were significantly faster in the presence of an ionic liquid.

In a posterior work, Freitas et al. [118] prepared a series of six composites of  $x\%$  HPA/BEA and compared them to six other composites of  $x\%$  HPA/Y ( $x = 10$  to 40 wt.%; zeolite beta and Y, with Si/Al = 12.5 and 2.6, respectively; HPA is HPW and HSiW). Besides structural and textural characterization, their acidity was investigated by microcalorimetric adsorption of pyridine in cyclohexane. It was observed that the supported catalysts present an acid strength lower than the pristine solids, which was expected by the leveling effect of the acidities. It is observed that protons of the HPA can interact much stronger with the surface sites of zeolites. However, even with this decrease, there were new sites with average strengths of  $-\Delta H = 125 \text{ kJ mol}^{-1}$ , which are suitable for the esterification reaction of *n*-butanol with acetic acid. A good correlation was observed between the catalytic activity of the composite materials with acidity results obtained by calorimetry. The catalysts that showed the strongest acid sites 39%HPW/BEA ( $-\Delta H = 144 \text{ kJ mol}^{-1}$ ), 40%HPW/Y ( $-\Delta H = 146 \text{ kJ mol}^{-1}$ ) and 44%HSiW/Y ( $-\Delta H = 143 \text{ kJ mol}^{-1}$ ) were the most active in the reaction, with conversions of 83, 78, and 66%, respectively, to butyl acetate under these conditions: molar ratio of 1:2 (acetic acid and *n*-butanol), 10 wt.% catalysts, and 1 h reaction.

Paiva et al. [149] have shown an interesting association of HPA and zeolites for catalysis. Therefore, zeolite Y (faujasite, Si/Al = 2.5) was changed by the incipient impregnation of HPW and HSiW forming  $x\%$  HPA/Y ( $x = 3, 6,$  and 12 wt.%), i.e., low loadings to improve the interaction between the phases and avoid leaching. The catalysts were characterized by various spectroscopic, morphological, thermal, and acidity by pyridine adsorption methods. Once again, the FT-IR spectra of pyridine adsorbed on the catalysts showed Brønsted and Lewis sites, with the former being gradually reduced in the intensity of the band as increased in the impregnated HPA. This is responsible for the strong interaction between the Keggin anion and the extraframework aluminum species on the zeolite Y surface. The formed solid acid composites revealed advantages over both pristine solids with suitable nature, strength, dispersion, and accessibility of the active sites. The application of these composites in the esterification of oleic acid with *n*-butanol formed butyl oleate, which is a fine chemical product that can be used in a variety of applications (e.g., plasticizers, lubricants). The catalysts exhibited high activities (high conversions and turnover number, TON), as well as a linear increase with HPA loading (Figure 8). The best catalyst (12%HPW/Y) showed 96% of oleic acid conversion and 100% selectivity to butyl oleate under very favorable reaction conditions (oleic acid: butanol molar ratio = 1:2; 10 wt.% of catalyst; 100 °C and 1 h reaction). There was no leaching of the Keggin phase detected, and it was reutilized in at least three reaction cycles with fair activity.

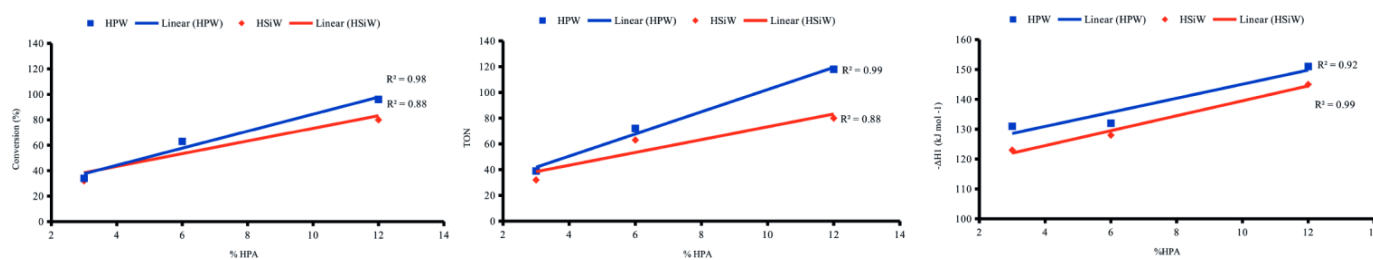


**Figure 8.** Correlations between conversion (%), TON, and  $\Delta H_1$  versus HPA loading. Adapted from reference [149]. Copyright © 2022 Elsevier, License Number: 5517671273883.

#### 4.4. Niobium-Based Catalysts

Braga et al. [150] synthesized niobium pentoxide supported on silica-alumina. This was the first time these catalysts were reported. They combine  $\text{Nb}_2\text{O}_5$ , which is considered a water-tolerant catalyst [125,151], with  $\text{SiO}_2\text{-Al}_2\text{O}_3$  (12 wt.% Al), which is a valuable support and industrial catalyst for different applications such as the FCC process. Thus, these catalysts ( $x\%$   $\text{Nb}_2\text{O}_5/\text{SiO}_2\text{-Al}_2\text{O}_3$ ,  $x = 2, 5, 10, 15, 20$ , and 25 wt.% of  $\text{Nb}_2\text{O}_5$ ) were prepared by aqueous solution impregnation using ammonium niobium oxalate and structurally characterized. Further, Braga et al. [152] compared the preparation of the same catalysts using grafting in  $\text{CH}_2\text{Cl}_2$  or ethanol solution with  $\text{NbCl}_5$  precursor. The catalytic materials were characterized by XRD, TG/DTG/DTA, FT-IR, DRIFTS, and FT-Raman. The results show that under calcination of 800 °C,  $\text{Nb}_2\text{O}_5$  has a strong interaction on the silica-alumina surface. It produced crystalline  $\text{Nb}_2\text{O}_5$  (T-phase) for the samples prepared by grafting, whereas T- and H-phases were obtained from the aqueous impregnation. This suggests higher stability of the catalysts formed by grafting. In addition, the acidity of these catalysts was estimated by calorimetric titration with pyridine in cyclohexane, with the catalysts activated at 300 °C. It was observed that the average values for all catalysts were approximately the same within  $\pm 2$  kJ mol<sup>-1</sup> for the same niobium pentoxide content, no matter the method of preparation. The average values for the enthalpies were:  $-\Delta H_1 = 104.6, 113.0, 96.2, \text{ and } 83.7$  kJ mol<sup>-1</sup> for 5, 10, 15, and 25 wt.% of  $\text{Nb}_2\text{O}_5$ , respectively. This order confirmed that the most acid catalysts are 10%  $\text{Nb}_2\text{O}_5/\text{SiO}_2\text{-Al}_2\text{O}_3$ , which agrees with other characterization methods that achieved the most active sites on the surface of these materials which were reached with 10–15 wt.% of  $\text{Nb}_2\text{O}_5$ . Thus, 10 wt.%  $\text{Nb}_2\text{O}_5/\text{SiO}_2\text{-Al}_2\text{O}_3$  was subjected to the esterification of acetic acid with ethanol, n-butanol, and isopentanol under these conditions: 2:1 molar ratio (acid: alcohol); 10 wt.% catalysts; temperature between 85 and 128 °C, according to the alcohol; 8 h reaction time. All yields were higher than 82%, which was considerably higher than the pristine solids.

Braga et al. [153] inserted CuO on those catalysts of  $\text{Nb}_2\text{O}_5/\text{SiO}_2\text{-Al}_2\text{O}_3$  since it is known that supported niobium pentoxide materials are effective catalysts for a variety of acid and redox reactions [154]. CuO and  $\text{Nb}_2\text{O}_5$  were supported on silica-alumina by two methods: co-impregnation and sequential impregnation, with CuO: $\text{Nb}_2\text{O}_5$  wt.% ratios = 1:10 and 1:1. The range studied was 5 to 25 wt.% of  $\text{Nb}_2\text{O}_5$ . The materials were characterized in their structure and applied in the oxidation of diesel soot using a model particulate (Printex<sup>®</sup> U). Based on the characterization results, it was indicated that the most promising materials could be generated by co-impregnation of the precursors with a 1:1 CuO: $\text{Nb}_2\text{O}_5$  wt.% ratio. In addition, Braga et al. [155] studied the acidity of these catalytic materials ( $\text{CuO}/\text{Nb}_2\text{O}_5/\text{SiO}_2\text{-Al}_2\text{O}_3$ ) with 1:1 CuO: $\text{Nb}_2\text{O}_5$  wt.% ratio prepared by simultaneous impregnation, in the range of 2 to 25 wt.% of each oxide. Their acidity was measured by calorimetric titrations with pyridine in cyclohexane slurries. The calorimetric curve (Figure 9) was divided into three regions, with complementary analysis using FT-IR: (i) in the first, the highest interaction average enthalpy ( $-\Delta H_1 = 94$  kJ mol<sup>-1</sup>) is related to Brønsted acid sites; (ii) in the middle, the average enthalpy is intermediate, i.e., values from  $50 < -\Delta H < 80$  kJ mol<sup>-1</sup>, which are related to the simultaneous interaction between pyridine and remaining Brønsted and Lewis acid sites; (iii) in the last region, pyridine

interacts with the Lewis acid sites, with lower average enthalpy ( $-\Delta H_2 = 58.7 \text{ kJ mol}^{-1}$ ), which started to react with pyridine just before all Brønsted were neutralized. A decrease was detected in Brønsted and a simultaneous increase in Lewis acid sites with the increased loadings of oxides. The most promising catalyst was that with the loading of 10 wt.% oxides since it has the highest number of acid sites ( $0.38 \text{ mmol g}^{-1}$ ) and the highest enthalpies of reaction with Brønsted and Lewis acid sites.

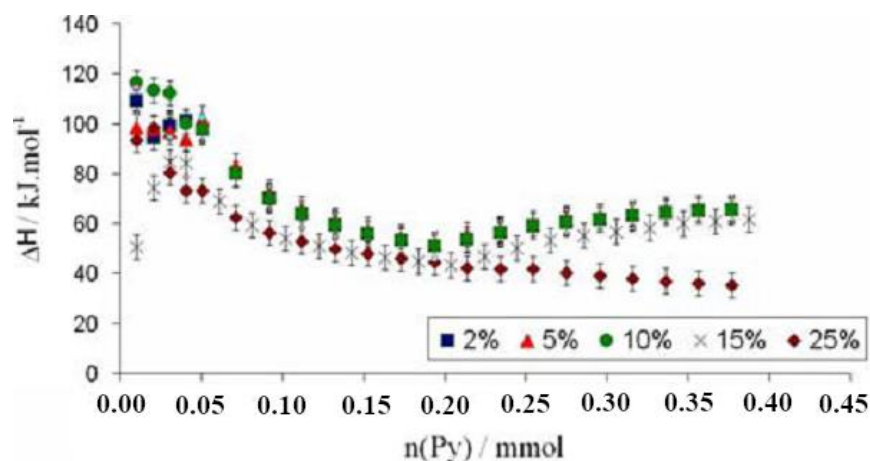


**Figure 9.** Calorimetric curves of CuO/Nb<sub>2</sub>O<sub>5</sub>/SiO<sub>2</sub>-Al<sub>2</sub>O<sub>3</sub> interaction with pyridine in cyclohexane. The error bars were set at  $\pm 5 \text{ kJ mol}^{-1}$  (two times the standard deviation). Adapted from reference [155]. Copyright © 2019 Springer, License Number: 5517680408110.

Valadares et al. [119] prepared dealuminated zeolite \*BEA (DB) from its protonic form (Si/Al = 12.5, calcined at 550 °C, 8 h) by solid state reaction with (NH<sub>4</sub>)<sub>2</sub>SiF<sub>6</sub>, removing 25% Al and promoting 13% Si insertion using a previous optimization process [156]. Then, this material (DB) was impregnated with ammonium niobium oxalate to produce 10, 18, and 25 wt.% of Nb<sub>2</sub>O<sub>5</sub> (x% Nb/DB), which were characterized by a number of methods and tested in their catalytic activity for ethanol and xylose dehydration. The catalyst 18% Nb/DB showed increased mesoporosity and external specific areas. In addition, a leveling effect in the number and strength of Brønsted and Lewis sites, which were obtained by microcalorimetry of pyridine adsorption, was observed. The 18% Nb/DB catalyst presented 97% selectivity for diethyl ether (DEE) with 61% conversion of ethanol (230 °C, minimum of 50 pulses) and 51% selectivity for furfural with 64% conversion of xylose (at 180 °C, water as the solvent). The acidity of the catalysts obtained by calorimetric titrations with pyridine (Figure 10) confirmed that initially, the probe interacts with the stronger Brønsted acid sites. In the middle of the curve, pyridine interacts with either Brønsted or Lewis sites, whereas at the end, pyridine reacts with weaker hydrogen bonding and Lewis sites. It was observed that increasing niobium loading on the support (x% Nb/DB) generally exhibited higher conversions, which was attributed to the gain of Lewis sites ( $-\Delta H_{2(\text{AVG})} = 45 \text{ kJ mol}^{-1}$ ). A combination of strength and more Lewis acid sites in the 18% Nb/DB catalyst was assigned as the main reason for the enhanced selectivity to DEE.

There are a variety of advantages of using biomass over fossil sources (e.g., abundant resources, natural replacement, lower pollution as fuels) [157,158]. In this sense, Lima et al. [159] selected a series of catalysts with different characteristics (zeolite Y, \*BEA, HZSM-5, SiO<sub>2</sub>-Al<sub>2</sub>O<sub>3</sub>, Nb<sub>2</sub>O<sub>5</sub>·nH<sub>2</sub>O, HPW, and HPW/Nb<sub>2</sub>O<sub>5</sub>) to be applied in the dehydration reaction of fructose in aqueous solution to 5-hydroxymethylfurfural (HMF). HMF is considered a platform molecule [157], i.e., it can be transformed into other important industrial chemicals. The acidity of these catalysts was previously obtained by the Cal-Ad method. In addition, the textural properties of these catalysts were obtained by N<sub>2</sub> adsorption at <sup>-196</sup> °C. It was possible to infer that the acidity parameters by themselves did not justify the order of selectivity to HMF or the fructose conversion. A combination between acidity and textural properties produced more reliable parameters for choosing

the best catalyst. The observed general order of selectivity to HMF was  $\text{Nb}_2\text{O}_5 > \text{HZSM-5} > 20\% \text{HPW}/\text{Nb}_2\text{O}_5 > \text{SiO}_2\text{-Al}_2\text{O}_3 > \text{HY} > \text{HBEA}$ . Thus, within the catalysts studied and the characterization methods used, it was possible to suggest the optimum parameters for the catalyst: acidic strength of  $80 < -\Delta H_1 < 100 \text{ kJ mol}^{-1}$ ; the total number of acid sites between  $0.20 < n_T < 0.30 \text{ mmol g}^{-1}$ ; density about one site  $\text{nm}^{-2}$  and mesoporous specific area about  $100 \text{ m}^2 \text{ g}^{-1}$ . Thus, it was clear that the reactivity of all tested catalysts toward fructose conversion could not be simplified based only on one parameter (e.g., strength, number, and density of acid sites). Textural parameters are key properties to enhance the selectivity of the HMF molecules.

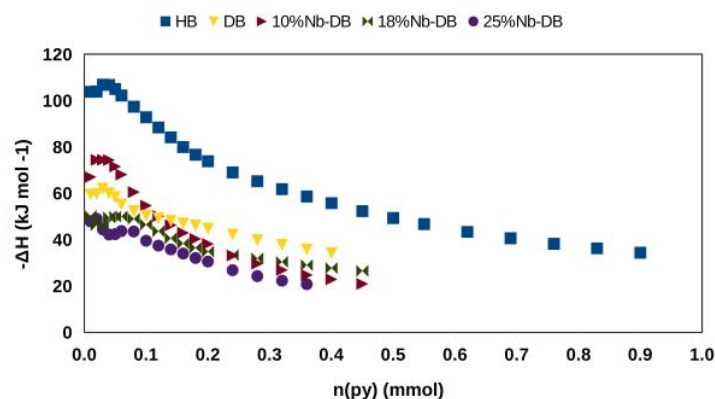


**Figure 10.** Calculated enthalpy difference ( $-\Delta H$ ) versus the number of moles of pyridine added during the calorimetric titration. Adapted from reference [119]. Copyright @ 2020 MDPI, License from Authors.

#### 4.5. Ordered Mesoporous Silica (OMS)

Alves et al. [160] synthesized ordered mesoporous silica (OMS) of type: FDU-12, MCM-41, SBA-16, and SBA-15 using verified methods in the literature [161–164] with the objective to study their surface hydroxyl groups depending on the pore structures. OMS is considered an essential and useful material for many applications (e.g., catalysis, adsorption, and controlled drug delivery) [165]. In this sense, FDU-12, SBA-16 (cubic), SBA-15, and MCM-41 (hexagonal pore structures) were chosen to observe this pore effect in their acidity. The last one had been studied by the Cal-Ad method comparatively to  $\text{SiO}_2$  and HZSM-5 by Braga et al. [163]. These materials were characterized by a number of conventional methods to show they had well-defined pores of long-range structural ordering, according to data in the literature. Donor–acceptor properties were obtained by calculation of the surface silanol ( $\text{Si-OH}$ ) and pyridine densities, whereas the nature of the silanol groups was confirmed as hydrogen bonding sites using FT-IR. Moreover, the reaction of ethanol dehydration, even at  $350 \text{ }^\circ\text{C}$ , did not show activity for those OMS, confirming that Brønsted and Lewis' sites were not present on these materials. The silanol groups could be explored by Py-TG and microcalorimetry of pyridine adsorption in cyclohexane slurry (Figure 11), which was able to quantitatively distinguish differences in the strength of the sites. The acidity order ( $-\Delta H_1$ ) was well correlated to the relative amount of silanol groups ( $\text{Si-OH}$ ) and pyridine on the surface of the OMS materials ( $\alpha_{\text{py}}$ ):  $\text{FDU-12} > \text{MCM-41} \geq \text{SBA-16} > \text{SBA-15}$ ;  $-\Delta H_1 = 74.5 > 66.8 > 66.1 > 36.8 \text{ kJ mol}^{-1}$ , respectively.

Microcalorimetry of pyridine adsorption could mark two types of active sites, which were stronger than those found on silica gel. The polar silanol groups formed inside the pores expose the OH mostly on the mesoporous walls because of the rigidity of their framework. An increase in the O–H bond distance takes place, which strengthens the hydrogen bonding interaction with pyridine. Thus, the slight differences in these distances possibly caused the difference in strength among the OMS materials.

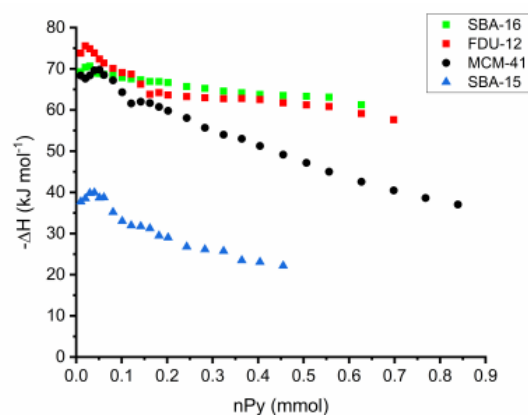


**Figure 11.** Calorimetric titration curves of OMS with pyridine in cyclohexane. Adapted from reference [160]. Copyright © 2021 Springer, License Number: 5517681068322.

A final summary of all thermodynamic data of these catalysts studied to date is provided in Table 3, either obtained by full Cal-Ad or only calorimetry in the liquid phase. This can facilitate finding a catalyst (organized by type) with its respective data of strength ( $-\Delta H$ ), number of sites ( $n$ ), and equilibrium constant ( $K$ ). Furthermore, Table 4 provides examples of some of these catalysts applied in a variety of reactions (e.g., alkylation, polymerization, dehydration, esterification), which may illustrate the potentiality of the Cal-Ad method to characterize acidity and correlate with activity.

**Table 3.** Solid acid catalysts characterized by Cal-Ad or only calorimetry. The data provide the conditions that each catalyst was activated before the respective measurement, and original reference for guidance. All reactions were solids with pyridine in cyclohexane solvent at  $25 \pm 1$  °C. Units are  $-\Delta H_i$  (kJ/mol);  $n_i$  (mmol/g);  $K_i$  (L/mol).

Catalyst (Activation)	$-\Delta H_1$	$n_1$	$K_1$	$-\Delta H_2$	$n_2$	$K_2$	Ref.
5% PdO/C	54.4	2.5	$2.5 \times 10^4$	41.8	3.2	$2.9 \times 10^2$	[87]
Silica <sup>(a)</sup>	52.7	0.86	$1.8 \times 10^4$	22.2	0.86	$3.2 \times 10^2$	[89]
Silica <sup>(b)</sup>	23.0	1.12	$2.5 \times 10^4$	13.4	1.30	$5.8 \times 10^2$	[89]
SZ <sup>(c)</sup>	130.5	0.027	$6.6 \times 10^9$	107.9	0.055	$3.0 \times 10^4$	[92]
SZ <sup>(d)</sup>	62.8						[92]
Pt-SZ <sup>(e)</sup>	125.5						[92]
SZ-Fe-Mn <sup>(e)</sup>	108.8						[92]
10.5% SG-W <sup>(b)</sup>	132.6	0.065	$6.8 \times 10^8$	67.8	0.41	$7.1 \times 10^2$	[93]
10% SG-WO <sub>3</sub> <sup>(f)</sup>	114.6	0.016	$1.2 \times 10^9$	74.5	0.24	$5.8 \times 10^3$	[93]
WO <sub>3</sub> <sup>(f)</sup>	41.8						[93]
H <sub>2</sub> WO <sub>4</sub>	71.1						[93]
SG-AlCl <sub>3</sub>	217.6	0.03		184.1	0.1		[94]
HZSM-5 <sup>(g)</sup>	176.1	0.042	$4.9 \times 10^6$		0.52	$2.3 \times 10^4$	[90]
TS-1 <sup>(h)</sup>	63.2	0.07	$6.7 \times 10^5$	2.4	0.31	$1.3 \times 10^4$	[107]
HY <sup>(g)</sup>	142.6	0.108	$2.1 \times 10^8$	74.1	0.22	$1.4 \times 10^6$	[108]
BEA <sup>(g)</sup>	148.0	0.15	$9 \times 10^6$	61.8	0.40	$6 \times 10^4$	[118]
DB <sup>(i)</sup>	60	0.16		49	0.24		[119]
MOR <sup>(g)</sup>	82.9	0.081	$2.7 \times 10^7$	36.7	0.422	$3.1 \times 10^4$	[114]
Ce/USY <sup>(i)</sup>	117.2	0.074	$8.7 \times 10^5$	87.9	1.117	$7.0 \times 10^3$	[112]
USY <sup>(i)</sup>	134.0	0.139	$2.0 \times 10^8$	101.5	0.737	$2.1 \times 10^6$	[112]
HPW <sup>(b)</sup>	136.8	0.08	$3.7 \times 10^5$	82.0	0.16	$2.9 \times 10^3$	[120]
12%HPW/Y <sup>(d)</sup>	151	0.32		36	0.10		[149]
40%HPW/Y <sup>(d)</sup>	146	0.08					[118]
39%HPW/BEA <sup>(d)</sup>	144	0.32					[118]
28%HSiW/Y <sup>(d)</sup>	123	0.06					[147]

Table 3. Cont.

Catalyst (Activation)	$-\Delta H_1$	$n_1$	$K_1$	$-\Delta H_2$	$n_2$	$K_2$	Ref.
8% HPW/SiO <sub>2</sub> <sup>(b)</sup>	87.9						[138]
15% HPW/SiO <sub>2</sub> <sup>(b)</sup>	100.4						[138]
20% HPW/SiO <sub>2</sub> <sup>(b)</sup>	108.8						[138]
25% HPW/SiO <sub>2</sub> <sup>(b)</sup>	116.7	0.102	$6.7 \times 10^5$	42.3	0.310	$3.8 \times 10^4$	[131]
20% HPW/Al <sub>2</sub> O <sub>3</sub> <sup>(b)</sup>	94.6	0.152	$1.2 \times 10^5$	50.2	0.20	$4.9 \times 10^3$	[140]
40% HPW/Al <sub>2</sub> O <sub>3</sub> <sup>(b)</sup>	75.3						[140]
$\gamma$ -Al <sub>2</sub> O <sub>3</sub> <sup>(d)</sup>	63.5	0.16		28.0	0.25		[140]
20% HPW/Nb <sub>2</sub> O <sub>5</sub> <sup>(b)</sup>	85	0.09		45	0.19		[159]
25% HPW/Nb <sub>2</sub> O <sub>5</sub> <sup>(b)</sup>	119.7	0.086	$8.8 \times 10^5$	43.5	0.191	$2.1 \times 10^5$	[141]
30% HPW/Nb <sub>2</sub> O <sub>5</sub> <sup>(b)</sup>	96.2						[141]
40% HPW/Nb <sub>2</sub> O <sub>5</sub> <sup>(b)</sup>	87.9						[141]
Nb <sub>2</sub> O <sub>5</sub> <sup>(d)</sup>	88	0.06		50	0.15		[159]
20% HPW/C <sup>(b)</sup>	93.7	0.129	$1.2 \times 10^7$	29.3	0.210	$8.6 \times 10^4$	[144]
20% HPW/C <sup>(h)</sup>	91	0.12					[144]
20% HPW/Al <sub>2</sub> O <sub>3</sub> <sup>(h)</sup>	97	0.12					[144]
20% HPW/SiO <sub>2</sub> <sup>(h)</sup>	110	0.09					[144]
C <sup>(b)</sup>	6						[144]
10%Nb-DB <sup>(i)</sup>	71	0.21		51	0.18		[119]
18%Nb-DB <sup>(i)</sup>	49	0.24		42	0.20		[119]
25%Nb-DB <sup>(i)</sup>	42	0.23		40	0.17		[119]
5% Nb <sub>2</sub> O <sub>5</sub> /Si-Al <sup>(d)</sup>	104.6						[152]
10% Nb <sub>2</sub> O <sub>5</sub> /Si-Al <sup>(d)</sup>	113.0						[152]
15% Nb <sub>2</sub> O <sub>5</sub> /Si-Al <sup>(d)</sup>	96.2						[152]
25% Nb <sub>2</sub> O <sub>5</sub> /Si-Al <sup>(d)</sup>	83.7						[152]
2% CuO/Nb <sub>2</sub> O <sub>5</sub> /Si-Al <sup>(d)</sup>	100.4			64.5			[155]
5% CuO/Nb <sub>2</sub> O <sub>5</sub> /Si-Al <sup>(d)</sup>	97.9			64.8			[155]
10% CuO/Nb <sub>2</sub> O <sub>5</sub> /Si-Al <sup>(d)</sup>	107.5			64.5			[155]
15% CuO/Nb <sub>2</sub> O <sub>5</sub> /Si-Al <sup>(d)</sup>	90.8			39.3			[155]
25% CuO/Nb <sub>2</sub> O <sub>5</sub> /Si-Al <sup>(d)</sup>	73.2			60.3			[155]
FDU-12 <sup>(b)</sup>	74.5	0.05		56.2	0.62		[160]
SBA-16 <sup>(b)</sup>	66.1	0.05		58.6	0.55		[160]
MCM-41 <sup>(b)</sup>	66.8	0.10		45.8	0.91		[160]
SBA-15 <sup>(b)</sup>	36.8	0.08		24.3	0.38		[160]

N.B. blank space means datum not available; DB = Dealuminated BEA zeolite; Si-Al = SiO<sub>2</sub>-Al<sub>2</sub>O<sub>3</sub>. <sup>a</sup> (vacuum, 28 °C); <sup>b</sup> (200 °C); <sup>c</sup> (600 °C); <sup>d</sup> (300 °C); <sup>e</sup> (600 °C); <sup>f</sup> (500 °C); <sup>g</sup> (450 °C); <sup>h</sup> (400 °C); <sup>i</sup> (550 °C).

Table 4. Examples of reactions correlating Cal-Ad data with conversion (C) and selectivity (S) for different catalysts.

Reaction	C (%) / S (%)	Catalyst	$-\Delta H_1$ (kJ/mol) / $n_T$ (mmol/g) <sup>a</sup>	Ref.
Ethylene/propene oligomerization	-	SG-AlCl <sub>2</sub>	217.6/0.13	[94]
Pentane isomerization	33% C	SZ	130.5/0.08	[92]
1-propanol dehydration	41% C	HPW	136.8/0.24	[120,123]
Benzene transalkylation with C9+ aromatics	3.9% S (xylenes)	15%HPW/SiO <sub>2</sub>	100.4/0.16	[138]
D,L-lactic acid polymerization	100% PLA <sup>b</sup> (ee 85% PLLA)	20%HPW/C	91/0.34	[143]
D,L-lactic acid polymerization	100% PLA <sup>b</sup> (ee 83% PLLA)	20%HPW/SiO <sub>2</sub>	110/0.40	[144]
D,L-lactic acid polymerization	100% PLA <sup>b</sup> (ee 95% PLLA)	20%HPW/Al <sub>2</sub> O <sub>3</sub>	97/0.35	[140]
				[144]

Table 4. Cont.

Reaction	C (%) / S (%)	Catalyst	$-\Delta H_1$ (kJ/mol) / $n_T$ (mmol/g) <sup>a</sup>	Ref.
Biginelli (MCR) <sup>c</sup>	99% yield	28%HSiW/Y	123/0.39	[147] [148]
Esterification of acetic acid with n-butanol (1 h)	77% C	40%HPW/Y	146/0.29	[147]
Esterification of oleic acid with n-butanol (1 h)	83% C	39%HPW/BEA	144/0.32	[118]
	96% C	12%HPW/Y	151/0.42	[149]
Esterification of acetic acid with ethanol, n-butanol and isopentanol (8 h)	83% C (ethanol) 87% C (n-butanol) 90% C (isopentanol)	10%Nb <sub>2</sub> O <sub>5</sub> /Si-Al	113/0.37	[152]
Dehydration of ethanol (300 °C)	100% C (ethylene)	HBEA	105/0.62	[156]
	65% C (ethylene)	DB	60/0.40	[119]
Dehydration of ethanol (230 °C)	97% S (DEE) <sup>d</sup>	18%Nb-DB	49/0.44	[119]
Dehydration of xylose (water, 180 °C)	51% C	18%Nb-DB	49/0.44	[119]
Dehydration of fructose (water, 120 °C)	64% S (furfural) 47.5% C 28.9% S (HMF) <sup>e</sup>	Nb <sub>2</sub> O <sub>5</sub>	88/0.21	[159]

<sup>a</sup> Enthalpy of the strongest sites ( $-\Delta H_1$ , kJ/mol) and total number of acid sites ( $n_T$ , mmol/g). <sup>b</sup> PLA: poly(lactic acid); ee: enantiomeric excess; PLLA: poly(L-lactic acid). <sup>c</sup> MCR (multicomponent reaction): benzaldehyde, urea and ethyl acetoacetate (equimolar quantities) and BMI.PF6 as solvent (1 h and 100 °C). <sup>d</sup> DEE: diethyl ether. <sup>e</sup> HMF: 5-hydroxymethylfurfural.

## 5. Conclusions

This review contains the fundamentals of the Cal-Ad method for a variety of catalysts. This method uses two independent experiments (calorimetry and adsorption), which coupled together and using a computational routine, can provide thermodynamic data such as enthalpy ( $\Delta H_i$ ), equilibrium constant ( $K_i$ ), and number of sites ( $n_i$ ) for a solid acid interacting with a basic probe. This method aims to offer an alternative for researchers to obtain acidity properties (e.g., strength, quantity, site distribution) using a direct measurement of their interaction enthalpies with pyridine and other bases. The characterized catalysts can be used as an acid strength reference scale for further applications. Many of them have been applied in a variety of reactions such as isomerization, oligomerization, polymerization, transalkylation, multicomponent (MCR), dehydration of alcohols (e.g., ethanol, 1-propanol), esterification, and dehydration of sugars (e.g., xylose, fructose). These are acidic-dependent reactions that have an optimal performance condition achieved by a suitable solid acid catalyst. Thus, the Cal-Ad analysis allows for catalyst selection and further design for different chemical reactions.

**Author Contributions:** D.d.S.V., J.O.C.d.F. and R.C.F. participated in initial conceptualization and revised articles in the literature. L.M.D. participated in initial conceptualization and revised the computational calculations involved in the method. S.C.L.D. and J.A.D. coordinated the work, participated in the conceptualization, wrote the first drafts of the paper, and coordinated the funding acquisition. All authors assisted equally in article manuscript revision and in discussion of the results. All authors have read and agreed to the published version of the manuscript.

**Funding:** This research was funded by Conselho Nacional de Desenvolvimento Científico e Tecnológico, CNPq (Grant Nos. 308693/2022-1, 307413/2021-7, and 141018/2020-8) and Coordenação de Aperfeiçoamento de Pessoal de Nível Superior, CAPES (Grant no. 001) for research and graduate student scholarships, and the financial support provided by Decanato de Pesquisa e Inovação, Instituto de Química/Universidade de Brasília, DPI/IQ/UnB, Ministério da Ciência, Tecnologia e Inovações/Conselho Nacional de Desenvolvimento Científico e Tecnológico, Fundação de Apoio a Pesquisa do Distrito Federal (FAPDF) (Grant No. 0193.00000229/2021-21, Projects 237/2021 and 302/2021), Fundação de Empreendimentos Científicos e Tecnológicos (FINATEC), Financiadora de

Estudos e Projetos, FINEP/CTPetro/CTInfra, and Petrobras. The APC was kindly provided by Chemistry (Voucher number fed677df370b96ca).

**Data Availability Statement:** All data can be accessed from the original cited references.

**Acknowledgments:** The authors would like to express their tribute, respect, and gratitude for Russel S. Drago (1928–1997), beloved friend and mentor of Cal-Ad method.

**Conflicts of Interest:** The authors declare no competing financial or any other conflicts of interest.

## References

1. Meschel, S.V. A brief history of heat measurements by calorimetry with emphasis on the thermochemistry. *Calphad* **2020**, *68*, 101714. [[CrossRef](#)]
2. Swenson, H.; Stadie, N.P. Langmuir's theory of adsorption: A centennial review. *Langmuir* **2019**, *35*, 5409–5426. [[CrossRef](#)] [[PubMed](#)]
3. Foo, K.Y.; Hameed, B.H. Insights into the modeling of adsorption isotherm systems. *Chem. Eng. J.* **2010**, *156*, 2–10. [[CrossRef](#)]
4. Housecroft, C.E.; Sharpe, A.G. *Inorganic Chemistry*, 2nd ed.; Pearson: London, UK, 2005; pp. 162–191.
5. Shriver, D.F.; Atkins, P.W.; Overton, T.L.; Rourke, J.P.; Weller, M.T.; Armstrong, F.A. *Química Inorgânica*, 4th ed.; Editora Bookman: São Paulo, Brazil, 2008; pp. 133–162.
6. Cotton, A.; Wilkinson, G.; Gaus, P. *Basic Inorganic Chemistry*, 3rd ed.; John Wiley & Sons: New York, NY, USA, 1994; pp. 206–225.
7. Huheey, J.E.; Keiter, E.A.; Keiter, R.L. *Inorganic Chemistry*, 4th ed.; Ed. Harper Collins: New York, NY, USA, 1993; pp. 318–358.
8. Jolly, W.L. *Modern Inorganic Chemistry*; McGraw Hill International Editions: Singapore, 1986; pp. 171–211.
9. Vogt, C.; Weckhuysen, B.M. The concept of active site in heterogeneous catalysis. *Nat. Rev. Chem.* **2022**, *6*, 89–111. [[CrossRef](#)] [[PubMed](#)]
10. Busca, G.; Gervasini, A. Solid acids, surface acidity and heterogeneous acid catalysis. Chapter one. *Adv. Catal.* **2020**, *67*, 1–90. [[CrossRef](#)]
11. Murzin, D.Y. Acid site density as a kinetic descriptor of catalytic reactions over zeolites. *Chemistry* **2022**, *4*, 1609–1623. [[CrossRef](#)]
12. Paenurk, E.; Kaupmees, K.; Himmel, D.; Kütt, A.; Kaljurand, I.; Koppel, I.A.; Krossing, I.; Leito, I. A unified view to Brønsted acidity scales: Do we need solvated protons? *Chem. Sci.* **2017**, *8*, 6964–6973. [[CrossRef](#)]
13. Dumeignil, F.; Paul, J.-F.; Paul, S. Heterogeneous catalysis with renewed attention: Principles, theories, and concepts. *J. Chem. Educ.* **2017**, *94*, 675–689. [[CrossRef](#)]
14. Védrine, J.C. Acid–base characterization of heterogeneous catalysts: An up-to-date overview. *Res. Chem. Intermed.* **2015**, *41*, 9387–9423. [[CrossRef](#)]
15. Moreno, E.L.; Rajagopal, K. Desafios da acidez na catálise em estado sólido. *Quim. Nova* **2009**, *32*, 538–542. [[CrossRef](#)]
16. Busca, G. Acid catalysts in industrial hydrocarbon chemistry. *Chem. Rev.* **2007**, *107*, 5366–5410. [[CrossRef](#)] [[PubMed](#)]
17. Zimmermann, Y.; Spange, S. Probing surface acidity, basicity, and dipolarity/polarizability of 12-tungstophosphoric acid by means of solvatochromic dyes. *New J. Chem.* **2002**, *26*, 1179–1184. [[CrossRef](#)]
18. Kijenski, J.; Baiker, A. Acidic sites on catalyst surfaces and their determination. *Catal. Today* **1989**, *5*, 1–120. [[CrossRef](#)]
19. Forni, L. Comparison of the methods for the determination of surface acidity of solid catalysts. *Catal. Rev. Sci. Eng.* **1974**, *8*, 65–115. [[CrossRef](#)]
20. Mirodatos, C.; Barthomeuf, D. Acidic and cracking properties of offretite. *J. Catal.* **1979**, *57*, 136–146. [[CrossRef](#)]
21. Parrilo, D.J.; Adamo, A.T.; Kokotailo, G.T.; Gorte, R.J. Amine adsorption in HZSM-5. *Appl. Catal.* **1990**, *67*, 107–118. [[CrossRef](#)]
22. Tittensor, J.G.; Gorte, R.J.; Chapman, D.M. Isopropylamine adsorption for the characterization of acid sites in silica-alumina catalysts. *J. Catal.* **1992**, *138*, 714–720. [[CrossRef](#)]
23. Lónyi, F.; Valyon, J. On the interpretation of the NH<sub>3</sub>-TPD patterns of H-ZSM-5 and H-mordenite. *Microporous Mesoporous Mater.* **2001**, *47*, 293–301. [[CrossRef](#)]
24. Martins, G.V.A.; Berlier, G.; Bisio, C.; Coluccia, S.; Pastore, H.O.; Marchese, L. Quantification of Brønsted acid sites in microporous catalysts by a combined FTIR and NH<sub>3</sub>-TPD study. *J. Phys. Chem. C* **2008**, *112*, 7193–7200. [[CrossRef](#)]
25. Luo, J.; Kamasamudram, K.; Currier, N.; Yezerets, A. NH<sub>3</sub>-TPD methodology for quantifying hydrothermal aging of Cu/SSZ-13 SCR catalysts. *Chem. Eng. Sci.* **2018**, *190*, 60–67. [[CrossRef](#)]
26. Shafei, E.N.; Masudi, A.; Yamani, Z.H.; Muraza, O. Acidity modifications of nanozeolite-Y for enhanced selectivity to olefins from the steam catalytic cracking of dodecane. *RSC Adv.* **2022**, *12*, 18274. [[CrossRef](#)] [[PubMed](#)]
27. Nunes, R.F.; Costa, D.; Ferraria, A.M.; Botelho do Rego, A.M.; Ribeiro, F.; Martins, Â.; Fernandes, A. Heterogenization of heteropolyacid with metal-based alumina supports for the guaiacol gas-phase hydrodeoxygenation. *Molecules* **2023**, *28*, 2245. [[CrossRef](#)] [[PubMed](#)]
28. Schmal, M. *Catálise Heterogênea*; Editora Synergia: Rio de Janeiro, Brazil, 2011; pp. 208–250.
29. Mackenzie, K.J.D.; Smith, M.E. *Multinuclear Solid-State NMR of Inorganic Materials*; Pergamon Materials Series: Oxford, UK, 2002; pp. 3–57.
30. Drago, R.S. *Physical Methods for Chemists*, 2nd ed.; Saunders College Publishing: New York, NY, USA, 1992; pp. 211–352.

31. Hennel, J.W.; Klinowski, J. Magic-Angle Spinning: A Historical Perspective. New Techniques in Solid-State NMR. In *Topics in Current Chemistry*; Klinowski, J., Ed.; Springer: Berlin/Heidelberg, Germany, 2005; Volume 246, pp. 1–14. [[CrossRef](#)]
32. Polenova, T.; Gupta, R.; Goldbourt, A. Magic Angle Spinning NMR Spectroscopy: A Versatile Technique for Structural and Dynamic Analysis of Solid-Phase Systems. *Anal. Chem.* **2015**, *87*, 5458–5469. [[CrossRef](#)] [[PubMed](#)]
33. Corma, A. Inorganic Solid Acids and Their Use in Acid-Catalyzed Hydrocarbon Reactions. *Chem. Rev.* **1995**, *95*, 559–614. [[CrossRef](#)]
34. Zheng, A.; Huang, S.-J.; Wang, Q.; Zhang, H.; Deng, F.; Liu, S.-B. Progress in development and application of solid-state NMR for solid acid catalysis. *Chin. J. Catal.* **2013**, *34*, 436–491. [[CrossRef](#)]
35. Zheng, A.; Li, S.; Liu, S.-B.; Deng, F. Acidic properties and structure–activity correlations of solid acid catalysts revealed by solid-state NMR spectroscopy. *Acc. Chem. Res.* **2016**, *49*, 655–663. [[CrossRef](#)]
36. Hunger, M. Multinuclear solid-state NMR studies of acidic and non-acidic hydroxyl protons in zeolites. *Solid State Nucl. Magn. Reson.* **1996**, *6*, 1–29. [[CrossRef](#)]
37. Jiang, Y.; Huang, J.; Dai, W.; Hunger, M. Solid-state nuclear magnetic resonance investigations of the nature, property, and activity of acid sites on solid catalysts. *Solid State Nucl. Magn. Reson.* **2011**, *39*, 116–141. [[CrossRef](#)]
38. Li, J.; Gao, M.; Yan, W.; Yu, J. Regulation of the Si/Al ratios and Al distributions of zeolites and their impact on properties. *Chem. Sci.* **2023**, *14*, 1935–1959. [[CrossRef](#)]
39. Reif, B.; Ashbrook, S.E.; Emsley, L.; Hong, M. Solid-state NMR spectroscopy. *Nat. Rev. Methods Prim.* **2021**, *1*, 2. [[CrossRef](#)]
40. Brouwer, D.H.; Brouwer, C.C.; Mesa, S.; Semelhago, C.A.; Steckley, E.E.; Sun, M.P.Y.; Mikolajewski, J.G.; Baerlocher, C. Solid-state  $^{29}\text{Si}$  NMR spectra of pure silica zeolites for the International Zeolite Association Database of Zeolite Structures. *Microporous Mesoporous Mater.* **2020**, *297*, 110000. [[CrossRef](#)]
41. Li, S.H.; Lafon, O.; Wang, W.Y.; Wang, Q.; Wang, X.X.; Li, Y.; Xu, J.; Deng, F. Recent advances of solid-state NMR spectroscopy for microporous materials. *Adv. Mater.* **2020**, *32*, 2002879. [[CrossRef](#)] [[PubMed](#)]
42. Wang, S.; He, Y.; Jiao, W.; Wang, J.; Fan, W. Recent experimental and theoretical studies on Al siting/acid site distribution in zeolite framework. *Curr. Opin. Chem. Eng.* **2019**, *23*, 146–154. [[CrossRef](#)]
43. Osegovic, J.P.; Drago, R.S. A solid acidity scale based on the  $^{31}\text{P}$  MAS-NMR shift of chemisorbed triethylphosphine Oxide. *J. Catal.* **1999**, *182*, 1–4. [[CrossRef](#)]
44. Alonso, B.; Klurb, I.; Massiotta, D. Studies of surfaces through molecular probe adsorption and solid-state NMR. *Chem. Commun.* **2002**, 804–805. [[CrossRef](#)]
45. Zheng, A.; Zhang, H.; Lu, X.; Liu, S.-B.; Deng, F. Theoretical predictions of  $^{31}\text{P}$  NMR chemical shift threshold of trimethylphosphine oxide adsorbed on solid acid catalysts. *J. Phys. Chem. B* **2008**, *112*, 4496–4505. [[CrossRef](#)]
46. Yi, X.; Ko, H.-H.; Deng, F.; Liu, S.-B.; Zheng, A. Solid-state  $^{31}\text{P}$  NMR mapping of active centers and relevant spatial correlations in solid acid catalysts. *Nat. Protoc.* **2020**, *15*, 3527–3555. [[CrossRef](#)]
47. Zasukhin, D.S.; Kasyanov, I.A.; Kolyagin, Y.G.; Bulygina, A.I.; Kharas, K.C.; Ivanova, I.I. Evaluation of zeolite acidity by  $^{31}\text{P}$  MAS NMR spectroscopy of adsorbed phosphine oxides: Quantitative or not? *ACS Omega* **2022**, *7*, 12318–12328. [[CrossRef](#)]
48. Okuhara, T.; Nishimura, T.; Watanabe, H.; Misono, M. Insoluble heteropoly compounds as highly active catalysts for liquid-phase reactions. *J. Mol. Catal.* **1992**, *74*, 247–256. [[CrossRef](#)]
49. Wu, Y.; Ye, X.; Yang, X.; Wang, X.; Chu, W.; Hu, Y. Heterogenization of heteropolyacids: A general discussion on the preparation of supported acid catalysts. *Ind. Eng. Chem. Res.* **1996**, *35*, 2546–2560. [[CrossRef](#)]
50. Uchida, S.; Inumaru, K.; Misono, M. States and dynamic behavior of protons and water molecules in  $\text{H}_3\text{PW}_{12}\text{O}_{40}$  pseudoliquid phase analyzed by solid-state MAS NMR. *J. Phys. Chem. B* **2000**, *104*, 8108–8115. [[CrossRef](#)]
51. De Mattos, F.C.G.; De Carvalho, E.N.C.B.; De Freitas, E.F.; Paiva, M.F.; Ghesti, G.F.; De Macedo, J.L.; Dias, S.C.L.; Dias, J.A. Acidity and characterization of 12-tungstophosphoric acid supported on silica-alumina. *J. Braz. Chem. Soc.* **2017**, *28*, 336–347. [[CrossRef](#)]
52. Rafiee, E.; Eavani, S. Heterogenization of heteropoly compounds: A review of their structure and synthesis. *RSC Adv.* **2016**, *6*, 46433–46466. [[CrossRef](#)]
53. Chorkendorff, I.; Niemantsverdriet, J.W. *Concepts of Modern Catalysis and Kinetics*; WILEY-VCH Verlag GmbH & Co. KGaA: Weinheim, The Netherlands, 2003; pp. 155–157.
54. Available online: [https://resources.perkinelmer.com/corporate/cmsresources/images/46-74388bro\\_60yearsinfraredspectroscopy.pdf](https://resources.perkinelmer.com/corporate/cmsresources/images/46-74388bro_60yearsinfraredspectroscopy.pdf) (accessed on 20 March 2023).
55. Vimont, A.; Travert, A.; Binet, C.; Pichon, C.; Mialane, P.; Sécheresse, F.; Lavalley, J.-C. Relationship between infrared spectra and stoichiometry of pyridine- $\text{H}_3\text{PW}_{12}\text{O}_{40}$  salts using a new TGA-infrared coupling. *J. Catal.* **2006**, *241*, 221–224. [[CrossRef](#)]
56. Katada, N. Analysis and interpretation of acidic nature of aluminosilicates. *Mol. Catal.* **2018**, *458*, 116–126. [[CrossRef](#)]
57. Perry, E.P. An infrared study of pyridine adsorbed on acidic solids. Characterization of surface acidity. *J. Catal.* **1963**, *2*, 371–379. [[CrossRef](#)]
58. Basila, M.R.; Kantner, T.R.; Rhee, K.H. The nature of the acidic sites on a silica-alumina. Characterization by infrared spectroscopic studies of trimethylamine and pyridine chemisorption. *J. Phys. Chem.* **1964**, *68*, 3197–3207. [[CrossRef](#)]
59. Hughes, T.R.; White, H.M. A Study of the surface structure of decationized Y zeolite by quantitative infrared spectroscopy. *J. Phys. Chem.* **1967**, *71*, 2192–2201. [[CrossRef](#)]
60. Emeis, C.A. Determination of integrated molar extinction coefficients for infrared absorption bands of pyridine adsorbed on solid acid catalysts. *J. Catal.* **1993**, *141*, 347–354. [[CrossRef](#)]

61. Sadowska, K.; Góra-Marek, K.; Datka, J. Accessibility of acid sites in hierarchical zeolites: Quantitative IR studies of pivalonitrile adsorption. *J. Phys. Chem. C* **2013**, *117*, 9237–9244. [[CrossRef](#)]
62. Mlekodaj, K.; Tarach, K.; Datka, J.; Góra-Marek, K.; Makowski, W. Porosity and accessibility of acid sites in desilicated ZSM-5 zeolites studied using adsorption of probe molecules. *Microporous Mesoporous Mater.* **2014**, *183*, 54–61. [[CrossRef](#)]
63. Hadjiivanov, K. Identification and characterization of surface hydroxyl groups by infrared spectroscopy. Chapter two. *Adv. Catal.* **2014**, *57*, 99–318. [[CrossRef](#)]
64. Adamson, A.W.; Gast, A.P. *Physical Chemistry of Surfaces*, 6th ed.; John Wiley & Sons, Inc.: New York, NY, USA, 2012; pp. 390–422.
65. Cardona-Martinez, N.; Dumesic, J. Applications of adsorption microcalorimetry to the study of heterogeneous catalysis. *Adv. Catal.* **1992**, *38*, 149–244. [[CrossRef](#)]
66. Solinas, V.; Ferino, I. Microcalorimetric characterisation of acid-basic catalysts. *Catal. Today* **1998**, *41*, 179–189. [[CrossRef](#)]
67. Auroux, A. Acidity characterization by microcalorimetry and relationship with reactivity. *Top. Catal.* **1997**, *4*, 71–89. [[CrossRef](#)]
68. Pierre Le Parlouër, P.L. Thermal Analysis and Calorimetry Techniques for Catalytic Investigations. In *Calorimetry and Thermal Methods in Catalysis*; Auroux, A., Ed.; Springer Series in Material Science; Springer: Berlin/Heidelberg, Germany, 2013; Volume 154, pp. 70–81. [[CrossRef](#)]
69. Védriane, J.C.; Auroux, A.; Dejaifve, P.; Ducarme, V.; Hoser, H.; Zhou, S. Catalytic and physical properties of phosphorus-modified ZSM-5 zeolite. *J. Catal.* **1982**, *73*, 147–160. [[CrossRef](#)]
70. Cardona-Martínez, N.; Dumesic, J.A. Acid strength of silica-alumina and silica studied by microcalorimetric measurements of pyridine adsorption. *J. Catal.* **1990**, *125*, 427–444. [[CrossRef](#)]
71. Cardona-Martínez, N.; Dumesic, J.A. Microcalorimetric measurements of basic molecule adsorption on silica and silica-alumina. *J. Catal.* **1991**, *128*, 23–33. [[CrossRef](#)]
72. Carniti, P.; Gervasini, A.; Biella, S.; Auroux, A. Intrinsic and effective acidity study of niobic acid and niobium phosphate by a multitechnique approach. *Chem. Mater.* **2005**, *17*, 6128–6136. [[CrossRef](#)]
73. Kozhevnikova, E.F.; Kozhevnikov, I.V. A calorimetric study of the acidity of bulk and silica-supported heteropoly acid H<sub>3</sub>PW<sub>12</sub>O<sub>40</sub>. *J. Catal.* **2004**, *224*, 164–169. [[CrossRef](#)]
74. Auroux, A.; Gervasini, A. Combined use of titration calorimetry and spectrofluorimetry for the screening of the acidity of solid catalysts in different liquids. *Thermochim. Acta* **2013**, *567*, 8–14. [[CrossRef](#)]
75. Stošić, D.; Bennici, S.; Sirotin, S.; Stelmachowski, P.; Couturier, J.-L.; Dubois, J.-L.; Travert, A.; Auroux, A. Examination of acid–base properties of solid catalysts for gas phase dehydration of glycerol: FTIR and adsorption microcalorimetry studies. *Catal. Today* **2014**, *226*, 167–175. [[CrossRef](#)]
76. Sánchez-Zambrano, K.S.; Vilarrasa-García, E.; Maia, D.A.S.; Bastos-Neto, M.; Rodríguez-Castellon, E.; Azevedo, D.C.S. Adsorption microcalorimetry as a tool in the characterization of amine-grafted mesoporous silicas for CO<sub>2</sub> capture. *Adsorption* **2020**, *26*, 165–175. [[CrossRef](#)]
77. Lund, C.R.F.; Tatarchuk, B.; Cardona-Martinez, N.; Hill, J.M.; Sanchez-Castillo, M.A.; Huber, G.W.; Roman-Leshkov, Y.; Simonetti, D.; Pagan-Torres, Y.; Schwartz, T.J. A Career in Catalysis: James A. Dumesic. *ACS Catal.* **2021**, *11*, 2310–2339. [[CrossRef](#)]
78. Drago, R.S. *Applications of Electrostatic-Covalent Models in Chemistry*; Surfside Scientific Publishers: Gainesville, FL, USA, 1994; pp. 1–308.
79. Pauling, L. The nature of the chemical bond. Application of results obtained from the quantum mechanics and from a theory of paramagnetic susceptibility to the structure of molecules. *J. Am. Chem. Soc.* **1931**, *53*, 1367–1400. [[CrossRef](#)]
80. Mulliken, R.S. Molecular compounds and their spectra II. *J. Am. Chem. Soc.* **1952**, *74*, 811–824. [[CrossRef](#)]
81. Fowkes, F.M.; McCarthy, D.C.; Tischler, D.O. *Polymer Science and Technology*; Plenum Press: New York, NY, USA, 1983; Volume 27, pp. 1–27.
82. Nozari, M.S.; Drago, R.S. Elimination of solvation contributions to the enthalpies of adduct formation in weakly polar solvents. II. Adducts of bis(hexafluoroacetylacetonato)copper(II). *Inorg. Chem.* **1972**, *11*, 280–283. [[CrossRef](#)]
83. Nozari, M.S.; Drago, R.S. Evaluation of models and effects contributing to solvent-transfer energies. *J. Am. Chem. Soc.* **1972**, *94*, 6877–6883. [[CrossRef](#)]
84. Drago, R.S.; Cundari, T.R.; Ferris, D.C. Structural and energetic analysis of gas-phase hydrated ammonium ions with relevance to the “anomalous” order in amine basicities. *J. Org. Chem.* **1989**, *54*, 1042–1047. [[CrossRef](#)]
85. Drago, R.S.; Ferris, D.C.; Wong, N. A method for the analysis and prediction of gas-phase ion-molecule enthalpies. *J. Am. Chem. Soc.* **1990**, *112*, 8953–8961. [[CrossRef](#)]
86. Webster, C.E.; Osegovic, J.P.; Scott, B.J.; Dias, S.C. A thermodynamic analysis of the Cal–Ad method with respect to gas–solid calorimetry. *Microporous Mesoporous Mater.* **1999**, *31*, 205–209. [[CrossRef](#)]
87. Lim, Y.Y.; Drago, R.S.; Babich, M.W.; Wong, N.; Doan, P.E. Thermodynamic Studies of Donor Binding to Heterogeneous. *J. Am. Chem. Soc.* **1987**, *109*, 169–174. [[CrossRef](#)]
88. Freitas, E.F. Reação de Esterificação e de Biginelli via Catalise por Polioxometalatos Impregnados em Zeólita Y. Ph.D. Dissertation, Universidade de Brasília, Brasília, Brazil, 2017.
89. Chronister, C.W.; Drago, R.S. Determination of Hydrogen-Bonding Acid Sites on Silica Using the Cal-Ad Method. *J. Am. Chem. Soc.* **1993**, *115*, 4793–4798. [[CrossRef](#)]
90. Drago, R.S.; Dias, S.C.; Torrealba, M.; Lima, L. Calorimetric and Spectroscopic Investigation of the Acidity of HZSM-5. *J. Am. Chem. Soc.* **1997**, *119*, 4444–4452. [[CrossRef](#)]

91. Anton, H.; Rorres, C. *Elementary Linear Algebra: Applications Version*, 11th ed.; John Wiley & Sons: Hoboken, NJ, USA, 2013; pp. 2–96.
92. Drago, R.S.; Kob, N. Acidity and Reactivity of Sulfated Zirconia and Metal-Doped Sulfated Zirconia. *J. Phys. Chem. B* **1997**, *101*, 3360–3364. [[CrossRef](#)]
93. Kob, N.; Drago, R.S.; Young, V. Preparation, Characterization, and Acidity of a Silica Gel/Tungsten Oxide Solid Acid. *Inorg. Chem.* **1997**, *36*, 5127–5131. [[CrossRef](#)]
94. Xu, T.; Kob, N.; Drago, R.S.; Nicholas, J.B.; Haw, J.F. A Solid Acid Catalyst at the Threshold of Superacid Strength: NMR, Calorimetry, and Density Functional Theory Studies of Silica-Supported Aluminum Chloride. *J. Am. Chem. Soc.* **1997**, *119*, 12231–12239. [[CrossRef](#)]
95. Drago, R.S.; Dias, J.A.; Maier, T.O. An acidity scale for Brønsted acids including  $H_3PW_{12}O_{40}$ . *J. Am. Chem. Soc.* **1997**, *119*, 7702–7710. [[CrossRef](#)]
96. Hench, L.L.; West, J.K. The sol-gel process. *Chem. Rev.* **1990**, *90*, 33–72. [[CrossRef](#)]
97. Jones, J.R. Review of bioactive glass: From Hench to hybrids. *Acta Biomater.* **2013**, *9*, 4457–4486. [[CrossRef](#)]
98. Gomes, L.S.; Furtado, A.C.R.; Souza, M.C. A Sílica e suas Particularidades. *Rev. Virtual Quim.* **2018**, *10*, 1018–1038. [[CrossRef](#)]
99. Gravelle, P.C. Calorimetry in adsorption and heterogeneous catalysis studies. *Catal. Rev.* **1977**, *16*, 37–110. [[CrossRef](#)]
100. Arnett, E.M.; Cassidy, K.F. A thermochemical comparison of silica with other homogeneous and heterogeneous acids. *Rev. Chem. Intermed.* **1988**, *9*, 27–64. [[CrossRef](#)]
101. Feher, F.J.; Newman, D.A. Enhanced silylation reactivity of a model for silica surfaces. *J. Am. Chem. Soc.* **1990**, *112*, 1931–1936. [[CrossRef](#)]
102. Hino, H.; Arata, K. Synthesis of solid superacid catalyst with acid strength of  $H_0 \leq -16.04$ . *J. Chem. Soc. Chem. Commun.* **1980**, 851–852. [[CrossRef](#)]
103. Rao, V.; Chary, K.; Durgakumari, V.; Narayanan, S. Catalytic alkylation of phenol with methanol: Factors influencing activities and selectivities: I. Effect of different acid sites evaluated by studying the behaviour of the catalysts:  $\gamma$ -alumina, nafion-H, silica-alumina and phosphoric acid. *Appl. Catal.* **1990**, *64*, 83–99. [[CrossRef](#)]
104. Bezouhanova, C.; Al-Zihari, M. Alkylation of phenol over simple oxides and supported vanadium oxides. *Appl. Catal.* **1990**, *61*, 89–97. [[CrossRef](#)]
105. Drago, R.S.; Getty, E.E. Preparation and Catalytic Activity of a New Solid Acid Catalyst. *J. Am. Chem. Soc.* **1988**, *110*, 3311–3312. [[CrossRef](#)]
106. Notari, B. Microporous crystalline titanium silicates. *Adv. Catal.* **1996**, *41*, 253–334. [[CrossRef](#)]
107. Drago, R.S.; Dias, S.C.; McGilvray, J.M.; Mateus, A.L.M.L. Acidity and hydrophobicity of TS-1. *J. Phys. Chem. B* **1998**, *102*, 1508–1514. [[CrossRef](#)]
108. Loureiro Dias, S.C.; de Macedo, J.L.; Dias, J.A. Acidity measurements of zeolite Y by adsorption of several probes. *Phys. Chem. Chem. Phys.* **2003**, *5*, 5574–5579. [[CrossRef](#)]
109. Puente, G.; Aguiar, E.F.S.; Zontin, F.M.Z.; Camorim, V.L.D.; Sedran, U. Influence of different rare earth ions on hydrogen transfer over Y zeolite. *Appl. Catal. A* **2000**, *197*, 41–46. [[CrossRef](#)]
110. Xue, M.; Chitrakar, R.; Sakane, K.; Hirotsu, T.; Ooi, K.; Yoshimura, Y.; Toba, M.; Feng, Q. Preparation of cerium-loaded Y-zeolites for removal of organic sulfur compounds from hydrodesulfurized gasoline and diesel oil. *J. Colloid Interface Sci.* **2006**, *298*, 535–542. [[CrossRef](#)] [[PubMed](#)]
111. Garcia, F.A.C.; Araújo, D.R.; Silva, J.C.M.; de Macedo, J.L.; Ghesti, G.F.; Dias, S.C.L.; Dias, J.A.; Filho, G.N.R. Effect of cerium loading on structure and morphology of modified Ce-USY zeolites. *J. Braz. Chem. Soc.* **2011**, *22*, 1894–1902. [[CrossRef](#)]
112. Ghesti, G.F.; de Macedo, J.L.; Parente, V.C.I.; Dias, J.A.; Dias, S.C.L. Investigation of pyridine sorption in USY and Ce/USY zeolites by liquid phase microcalorimetry and thermogravimetry studies. *Microporous Mesoporous Mater.* **2007**, *100*, 27–34. [[CrossRef](#)]
113. Webster, C.E.; Cottone, A.; Drago, R.S. Multiple equilibrium analysis description of adsorption on Na–Mordenite and H–Mordenite. *J. Am. Chem. Soc.* **1999**, *121*, 12127–12139. [[CrossRef](#)]
114. de Macedo, J.L.; Dias, S.C.L.; Dias, J.A. Multiple adsorption process description of zeolite mordenite acidity. *Microporous Mesoporous Mater.* **2004**, *72*, 119–125. [[CrossRef](#)]
115. Lu, T.; Yan, W.; Xu, R. Chiral zeolite beta: Structure, synthesis, and application. *Inorg. Chem. Front.* **2019**, *6*, 1938–1951. [[CrossRef](#)]
116. de Macedo, J.L.; Ghesti, G.F.; Dias, J.A.; Dias, S.C.L. Liquid phase calorimetry and adsorption analyses of zeolite beta acidity. *Phys. Chem. Chem. Phys.* **2008**, *10*, 1584–1592. [[CrossRef](#)]
117. Kikhtyanin, O.; Bulánek, R.; Frolich, K.; Cejka, J.; Kubicka, D. Aldol condensation of furfural with acetone over ion-exchanged and impregnated potassium BEA zeolites. *J. Mol. Catal. A* **2016**, *424*, 358–368. [[CrossRef](#)]
118. Freitas, E.F.; Araújo, A.A.L.; Paiva, M.F.; Dias, S.C.L.; Dias, J.A. Comparative acidity of BEA and Y zeolite composites with 12-tungstophosphoric and 12-tungstosilicic acids. *Mol. Catal.* **2018**, *458*, 152–160. [[CrossRef](#)]
119. Valadares, D.S.; Clemente, M.C.H.; de Freitas, E.F.; Martins, G.A.V.; Dias, J.A.; Dias, S.C.L. Niobium on BEA dealuminated zeolite for high selectivity dehydration reactions of ethanol and xylose into diethyl ether and furfural. *Nanomaterials* **2020**, *10*, 1269. [[CrossRef](#)] [[PubMed](#)]
120. Dias, J.A.; Osegovic, J.P.; Drago, R.S. The solid acidity of 12-tungstophosphoric acid. *J. Catal.* **1999**, *183*, 83–90. [[CrossRef](#)]
121. Misono, M. Heterogeneous catalysis by heteropoly compounds of molybdenum and tungsten. *Catal. Rev. Sci. Eng.* **1987**, *29*, 269–321. [[CrossRef](#)]

122. Lee, K.Y.; Arai, T.; Nakata, S.; Asaoka, S.; Okuhara, T.; Misono, M. Catalysis by heteropoly compounds. 20. An NMR study of ethanol dehydration in the pseudoliquid phase of 12-tungstophosphoric acid. *J. Am. Chem. Soc.* **1992**, *114*, 2836–2842. [[CrossRef](#)]
123. Dias, J.A.; Dias, S.C.L.; Kob, N.E. Dehydration of 1-propanol using  $H_3PW_{12}O_{40}$  as catalyst. *J. Chem. Soc. Dalton Trans.* **2001**, 228–231. [[CrossRef](#)]
124. Dias, J.A.; Caliman, E.; Dias, S.C.L. Effects of cesium ion exchange on acidity of 12-tungstophosphoric acid. *Microporous Mesoporous Mater.* **2004**, *76*, 221–232. [[CrossRef](#)]
125. Okuhara, T. Water-Tolerant Solid Acid Catalysts. *Chem. Rev.* **2002**, *102*, 3641–3666. [[CrossRef](#)]
126. Corma, A.; Martínez, A.; Martínez, C. Acidic  $Cs^+$ ,  $NH_4^+$ , and  $K^+$  Salts of 12-tungstophosphoric acid as solid catalysts for isobutane/2-butene alkylation. *J. Catal.* **1996**, *164*, 422–432. [[CrossRef](#)]
127. da Silva, M.J.; Rodrigues, A.A.; Lopes, N.P.G. Cesium heteropolyacid salts: Synthesis, characterization and activity of the solid and versatile heterogeneous catalysts. *Chemistry* **2023**, *5*, 662–690. [[CrossRef](#)]
128. Nishimura, T.; Okuhara, T.; Misono, M. High catalytic activity of an insoluble acidic caesium salt of dodecatungstophosphoric acid for liquid-phase alkylation. *Appl. Catal.* **1991**, *73*, L7–L11. [[CrossRef](#)]
129. Dias, J.A.; Dias, S.C.L.; de Macedo, J.L. Effect of acidity, structure and stability of supported 12-tungstophosphoric acid on catalytic reactions. In *Environmentally Benign Catalysts for Clean Organic Reactions*; Patel, A., Ed.; Springer: London, UK, 2013; pp. 165–187. [[CrossRef](#)]
130. Rafiee, E.; Zolfaghari, Z.; Joshaghani, M.; Eavani, S. Facile condensation of indole with benzaldehyde over Keggin-type heteropoly compounds: An initial effort toward catalyst design. *Appl. Catal. A* **2009**, *365*, 287–291. [[CrossRef](#)]
131. Dias, J.A.; Caliman, E.; Dias, S.C.L.; Paulo, M.; de Souza, A.T.C.P. Preparation and characterization of supported  $H_3PW_{12}O_{40}$  on silica gel: A potential catalyst for green chemistry processes. *Catal. Today* **2003**, *85*, 39–48. [[CrossRef](#)]
132. Misono, M.; Inui, T. New catalytic technologies in Japan. *Catal. Today* **1999**, *51*, 369–375. [[CrossRef](#)]
133. Misono, M.; Ono, I.; Koyano, G.; Aoshima, A. Heteropolyacids. Versatile green catalysts usable in a variety of reaction media. *Pure Appl. Chem.* **2000**, *72*, 1305–1311. [[CrossRef](#)]
134. Kozhevnikov, I.V. (Ed.) *Catalysts for Fine Chemical Synthesis Catalysis by Polyoxometalates*; John Wiley & Sons Ltd.: Chichester, UK, 2002; Volume 2, pp. 1–42.
135. Zhang, Q.; Liu, X.; Deng, T.; Zhang, Y.; Ma, P. Recent progress on heteropolyacids for green fuels synthesis. *Curr. Green Chem.* **2019**, *7*, 267–281. [[CrossRef](#)]
136. Na, K. Synthesis and application of zeolite catalysts. *Catalysts* **2021**, *11*, 685. [[CrossRef](#)]
137. Escobar, A.M.; Blustein, G.; Luque, R.; Romanelli, G.P. Recent applications of heteropolyacids and related compounds in heterocycle synthesis. Contributions between 2010 and 2020. *Catalysts* **2021**, *11*, 291. [[CrossRef](#)]
138. Dias, J.A.; Rangel, M.C.; Dias, S.C.L.; Caliman, E.; Garcia, F.A.C. Benzene transalkylation with C9+ aromatics over supported 12-tungstophosphoric acid on silica catalysts. *Appl. Catal. A* **2007**, *328*, 189–194. [[CrossRef](#)]
139. Sotelo, J.L.; Calvo, L.; Velázquez, P.; Capilla, D.; Carvani, F.; Bolognini, M. A comparative study on the transalkylation of diisopropylbenzene with benzene over several zeolitic materials in supercritical  $CO_2$  and liquid phase. *Appl. Catal. A* **2006**, *312*, 194–201. [[CrossRef](#)]
140. Caliman, E.; Dias, J.A.; Dias, S.C.L.; Prado, A.G.S. Solvent effect on the preparation of  $H_3PW_{12}O_{40}$  supported on alumina. *Catal. Today* **2005**, *107–108*, 816–825. [[CrossRef](#)]
141. Caliman, E.; Dias, J.A.; Dias, S.C.L.; Garcia, F.A.C.; de Macedo, J.L.; Almeida, L.S. Preparation and characterization of  $H_3PW_{12}O_{40}$  supported on niobia. *Microporous Mesoporous Mater.* **2010**, *132*, 103–111. [[CrossRef](#)]
142. Lefebvre, F.; Dupont, P.; Auroux, A. Study of the acidity of  $H_3PW_{12}O_{40}$  supported on activated carbon by microcalorimetry and methanol dehydration reaction. *React. Kinet. Catal. Lett.* **1995**, *55*, 3. [[CrossRef](#)]
143. Chafran, L.S.; Campos, J.M.C.; Santos, J.S.; Sales, M.J.A.; Dias, S.C.L.; Dias, J.A. Synthesis of poly(lactic acid) by heterogeneous acid catalysis from D,L-lactic acid. *J. Polym. Res.* **2016**, *23*, 107. [[CrossRef](#)]
144. Chafran, L.S.; Paiva, M.F.; França, J.O.C.; Sales, M.J.A.; Dias, S.C.L.; Dias, J.A. Preparation of PLA blends by polycondensation of D,L-lactic acid using supported 12-tungstophosphoric acid as a heterogeneous catalyst. *Heliyon* **2019**, *5*, e01810. [[CrossRef](#)]
145. Rosenboom, J.-G.; Langer, R.; Traverso, G. Bioplastics for a circular economy. *Nat. Rev. Mater.* **2022**, *7*, 117–137. [[CrossRef](#)] [[PubMed](#)]
146. de França, J.O.C.; da Silva Valadares, D.; Paiva, M.F.; Dias, S.C.L.; Dias, J.A. Polymers based on PLA from synthesis using D,L-lactic acid (or racemic lactide) and some biomedical applications: A short review. *Polymers* **2022**, *14*, 2317. [[CrossRef](#)]
147. Freitas, E.F.; Paiva, M.F.; Dias, S.C.L.; Dias, J.A. Generation and characterization of catalytically active sites of heteropolyacids on zeolite Y for liquid-phase esterification. *Catal. Today* **2017**, *289*, 70–77. [[CrossRef](#)]
148. Freitas, E.F.; Souza, R.Y.; Passos, S.T.A.; Dias, J.A.; Dias, S.C.L.; Neto, B.A.D. Tuning the Biginelli reaction mechanism by the ionic liquid effect: The combined role of supported heteropolyacid derivatives and acidic strength. *RSC Adv.* **2019**, *9*, 27125–27135. [[CrossRef](#)]
149. Paiva, M.F.; Freitas, E.F.; de França, J.O.C.; da Silva Valadares, D.; Dias, S.C.L.; Dias, J.A. Structural and acidity analysis of heteropolyacids supported on faujasite zeolite and its effect in the esterification of oleic acid and n-butanol. *Mol. Catal.* **2022**, *532*, 112737. [[CrossRef](#)]
150. Braga, V.S.; Dias, J.A.; Dias, S.C.L.; Macedo, J.L. Catalyst materials based on  $Nb_2O_5$  supported on  $SiO_2-Al_2O_3$ : preparation and structural characterization. *Chem. Mater.* **2005**, *17*, 690–695. [[CrossRef](#)]

151. Nakajima, K.; Baba, Y.; Noma, R.; Kitano, M.; Kondo, J.N.; Hayashi, S.; Hara, M. Nb<sub>2</sub>O<sub>5</sub>·nH<sub>2</sub>O as a heterogeneous catalyst with water-tolerant Lewis acid sites. *J. Am. Chem. Soc.* **2011**, *133*, 4224–4227. [[CrossRef](#)] [[PubMed](#)]
152. Braga, V.S.; Barros, I.C.L.; Garcia, F.A.C.; Dias, S.C.L.; Dias, J.A. Esterification of acetic acid with alcohols using supported niobium pentoxide on silica–alumina catalysts. *Catal. Today* **2008**, *133–135*, 106–112. [[CrossRef](#)]
153. Braga, V.S.; Garcia, F.A.C.; Dias, S.C.L.; Dias, J.A. Copper oxide and niobium pentoxide supported on silica-alumina: Synthesis, characterization, and application on diesel soot oxidation. *J. Catal.* **2007**, *247*, 68–77. [[CrossRef](#)]
154. Nowak, I.; Ziolk, M. Niobium compounds: Preparation, characterization, and application in heterogeneous catalysis. *Chem. Rev.* **1999**, *99*, 3603–3624. [[CrossRef](#)]
155. Garcia, F.A.C.; Braga, V.S.; Silva, J.C.M.; Dias, J.A.; Dias, S.C.L.; Davo, J.L.B. Acidic characterization of copper oxide and niobium pentoxide supported on silica–alumina. *Catal. Lett.* **2007**, *119*, 101–107. [[CrossRef](#)]
156. Clemente, M.C.H.; Valadares, D.S.; Lacava, A.B.; Barbosa, L.S.; Martins, G.A.V.; Dias, J.A.; Dias, S.C.L. Catalytic transformation conditions of ethanol on dealuminated BEA zeolites. *J. Braz. Chem. Soc.* **2019**, *30*, 2182–2190. [[CrossRef](#)]
157. van Putten, R.-J.; van der Waal, J.C.; de Jong, E.; Rasrendra, C.B.; Heeres, H.J.; de Vries, J.G. Hydroxymethylfurfural, a versatile platform chemical made from renewable resources. *Chem. Rev.* **2013**, *113*, 1499–1597. [[CrossRef](#)]
158. Shahbeik, H.; Peng, W.; Panahi, H.K.S.; Dehghani, M.; Guillemin, G.J.; Fallahi, A.; Amiri, H.; Rehan, M.; Raikwar, D.; Latine, H.; et al. Synthesis of liquid biofuels from biomass by hydrothermal gasification: A critical review. *Renew. Sustain. Energy Rev.* **2022**, *167*, 112833. [[CrossRef](#)]
159. Lima, J.P.V.; Campos, P.T.A.; Paiva, M.F.; Linares, J.J.; Dias, S.C.L.; Dias, J.A. Dehydration of fructose to 5-hydroxymethylfurfural: Effects of acidity and porosity of different catalysts in the conversion, selectivity, and yield. *Chemistry* **2021**, *3*, 1189–1202. [[CrossRef](#)]
160. Alves, M.R.; Paiva, M.F.; Campos, P.T.A.; de Freitas, E.F.; Clemente, M.C.H.; Martins, G.A.V.; Silveira, A.T.; da Silva, L.C.C.; Fantini, M.C.A.; Dias, S.C.L.; et al. Accessibility and strength of H-acceptor hydroxyls of ordered mesoporous silicas probed by pyridine donor. *J. Porous Mater.* **2020**, *28*, 323–335. [[CrossRef](#)]
161. Meynen, V.; Cool, P.; Vansant, E.F. Verified syntheses of mesoporous materials. *Microporous Mesoporous Mater.* **2009**, *125*, 170–223. [[CrossRef](#)]
162. Zhao, D. Triblock copolymer syntheses of mesoporous silica with periodic 50 to 300 angstrom pores. *Science* **1998**, *279*, 548–552. [[CrossRef](#)] [[PubMed](#)]
163. Braga, P.R.S.; Costa, A.A.; de Macedo, J.L.; Ghesti, G.F.; de Souza, M.P.; Dias, J.A.; Dias, S.C.L. Liquid phase calorimetric-adsorption analysis of Si-MCM-41: Evidence of strong hydrogen-bonding sites. *Microporous Mesoporous Mater.* **2011**, *139*, 74–80. [[CrossRef](#)]
164. Fan, J.; Yu, C.; Gao, F.; Lei, J.; Tian, B.; Wang, L.; Luo, Q.; Tu, B.; Zhou, W.; Zhao, D. Cubic mesoporous silica with large controllable entrance sizes and advanced adsorption properties. *Angew. Chem. Int. Ed.* **2003**, *42*, 3146–3150. [[CrossRef](#)]
165. Schwanke, A.J.; Santos, A.P.B.; Bieseki, L.; Campos, P.R.P.; Pergher, S.B.C. *Materiais Mesoporosos: Um Caminho Acessível*; Editora da UFRN–Edufrn: Natal, Brazil, 2016; pp. 1–50.

**Disclaimer/Publisher’s Note:** The statements, opinions and data contained in all publications are solely those of the individual author(s) and contributor(s) and not of MDPI and/or the editor(s). MDPI and/or the editor(s) disclaim responsibility for any injury to people or property resulting from any ideas, methods, instructions or products referred to in the content.